FINAL REPORT

Development and Testing of an Engineering Prototype for a Marine Version of the Berkeley Unexploded Ordnance Discriminator (BUD)

SERDP Project MR-2228

JUNE 2013

H. Frank Morrison
Marine Advanced Research, Inc.

SERDP
DOD ▪ EPA ▪ DOE

Report Documentation Page

Form Approved
OMB No. 0704-0188

1. REPORT DATE	2. REPORT TYPE	3. DATES COVERED
JUN 2013		**00-00-2013 to 00-00-2013**

4. TITLE AND SUBTITLE	5a. CONTRACT NUMBER
Development and Testing of an Engineering Prototype for a Marine Version of the Berkeley Unexploded Ordnance Discriminator (BUD)	5b. GRANT NUMBER
	5c. PROGRAM ELEMENT NUMBER
6. AUTHOR(S)	5d. PROJECT NUMBER
	5e. TASK NUMBER
	5f. WORK UNIT NUMBER
7. PERFORMING ORGANIZATION NAME(S) AND ADDRESS(ES) **Marine Advanced Research, Inc.,El Cerrito,CA,94530**	8. PERFORMING ORGANIZATION REPORT NUMBER
9. SPONSORING/MONITORING AGENCY NAME(S) AND ADDRESS(ES)	10. SPONSOR/MONITOR'S ACRONYM(S)
	11. SPONSOR/MONITOR'S REPORT NUMBER(S)

12. DISTRIBUTION/AVAILABILITY STATEMENT
Approved for public release; distribution unlimited

13. SUPPLEMENTARY NOTES

14. ABSTRACT

A marine version of the Berkeley Unexploded Ordnance Discriminator [BUD] has been built and tested in shallow seawater. The system was built in response to a need to develop a geophysical system for detecting and characterizing UXO in the marine environment. Such a system must detect a metallic object, provide its depth and symmetry properties that allow it to be identified as an intact UXO. A three-component transmitter is mounted on a planar base and four threecomponent receivers are mounted on the same base and on the corners of a square pattern centered on the transmitter. Differences in field at symmetrically located receivers cancel the response of the seawater and of the air-sea interface above the system. New ferrite-cored induction coils coupled with a feedback amplifier scheme provide high stability and a critically damped response. The coils are mounted in rigid blocks to provide three-component sensor modules. A first stage of amplification at the sensors provides a high level signal from a low impedance source to carry the signals, without added coupling noise, over cables to differencing amplifiers in the data acquisition module. The current pulse in the transmitter coils is a bipolar half-sine of 5 msec. duration with a repetition rate of 12.5 Hz. A new pulser, based on the BUD pulser provides a peak moment of 2000 Amp. Turns M2 with current pulses of 200 A and a net power consumption of 400 Watts. Tests of the prototype on land and in 5 m of seawater showed that the system clearly detected a 6 inch (152.4 mm) steel test ball to over 57 cm depth and that the test ball yielded identical transients in air and seawater showing that the effects of the seawater and the air-sea interface were canceled in the new configuration.

15. SUBJECT TERMS

16. SECURITY CLASSIFICATION OF:			17. LIMITATION OF ABSTRACT	18. NUMBER OF PAGES	19a. NAME OF RESPONSIBLE PERSON
a. REPORT	b. ABSTRACT	c. THIS PAGE			
unclassified	**unclassified**	**unclassified**	**Same as Report (SAR)**	**50**	

TABLE OF CONTENTS

Acronyms

ADC	Analog to digital converter
BUD	Berkeley Unexploded Ordnance Discriminator
FPGA	Field programmable gate array
LBL	Lawrence Berkeley National Laboratory
MBUD	Marine version of BUD
UXO	Unexploded ordnance

Abstract

A marine version of the Berkeley Unexploded Ordnance Discriminator [BUD] has been built and tested in shallow seawater. The system was built in response to a need to develop a geophysical system for detecting and characterizing UXO in the marine environment. Such a system must detect a metallic object, provide its depth and symmetry properties that allow it to be identified as an intact UXO.

A three-component transmitter is mounted on a planar base and four three-component receivers are mounted on the same base and on the corners of a square pattern centered on the transmitter. Differences in field at symmetrically located receivers cancel the response of the seawater and of the air-sea interface above the system.

New ferrite-cored induction coils coupled with a feedback amplifier scheme provide high stability and a critically damped response. The coils are mounted in rigid blocks to provide three-component sensor modules. A first stage of amplification at the sensors provides a high level signal from a low impedance source to carry the signals, without added coupling noise, over cables to differencing amplifiers in the data acquisition module.

The current pulse in the transmitter coils is a bipolar half-sine of 5 msec. duration with a repetition rate of 12.5 Hz. A new pulser, based on the BUD pulser provides a peak moment of 2000 Amp. Turns M^2 with current pulses of 200 A and a net power consumption of 400 Watts.

Tests of the prototype on land and in 5 m of seawater showed that the system clearly detected a 6 inch (152.4 mm) steel test ball to over 57 cm depth and that the test ball yielded identical transients in air and seawater showing that the effects of the seawater and the air-sea interface were canceled in the new configuration.

Objective

The objective of this project has been to develop and test an engineering prototype of a marine version of the Berkeley Unexploded Ordnance Discriminator, BUD. There is a pressing need to develop a geophysical system for detecting and characterizing UXO in the marine environment. Attempts to date to adapt land-based electromagnetic (EM) systems to the marine environment have demonstrated inferior performance compared to their relative success on land. One such system is the Berkeley Unexploded Ordnance Discriminator (BUD) that has demonstrated better than 98% identification of UXO targets at four prove-out sites in the US. BUD has a fundamental transmitter-receiver configuration that inherently cancels the seawater response and this project has resulted in a modified BUD system that is optimized for marine use. The marine version that has been developed will henceforth be referred to as MBUD.

Background

The Berkeley unexploded ordnance discriminator (BUD) was designed from first principles using numerical models of simple shapes to determine the optimum configuration of transmitters and receivers needed to obtain the principal polarizabilities of a buried conductor. The goal was to use the symmetry properties of intact UXO to distinguish them from scrap.

BUD was designed for transient measurements: the secondary fields from the body were measured after the primary energizing magnetic field pulse (in this case series of alternating polarity half sine pulses) was terminated. Generally transient methods are used in EM systems where the transmitter and receiver are close together and the desired secondary fields from a target are very small compared to the direct primary field but are easily measured after the primary field is turned off. It was found that if a target body is illuminated with fields of different polarizations, provided by three orthogonal loop transmitters, and multiple transient field measurements are made with receivers close to the system, then the three orthogonal equivalent dipole polarizabilities of the target can be determined. A complete theoretical explanation can be found in published papers 2), 5), 6), 7), 8), 9), and 10) (in Literature Cited). BUD has been successfully demonstrated at a number of munitions sites around the country. Its fundamental configuration can be modified so that it will function in seawater almost as well as it does on land. It avoids a fundamental problem that has not been addressed by other marine electromagnetic UXO systems that have simply been waterproofed versions of land-based systems.

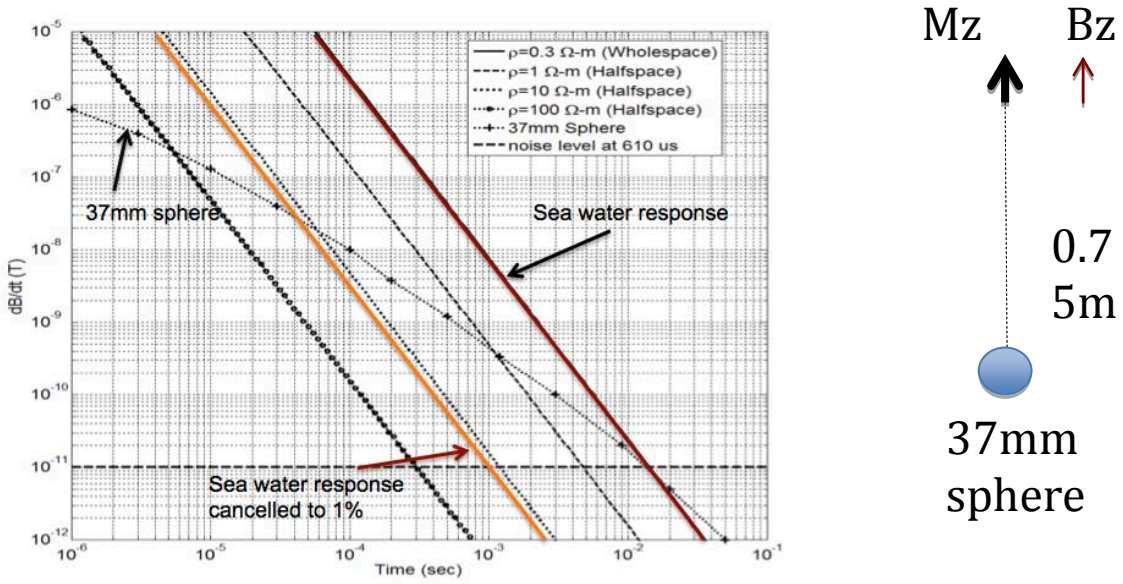

Figure 1

The fundamental problem with marine detection/discrimination is that the response of the seawater itself is comparable to, or larger than, the response of the target. The problem is illustrated in Figure 1 for the simple situation involving a vertical magnetic dipole source, Mz, a 37mm steel sphere target and a receiver, Bz, close to the transmitter. This somewhat extreme example shows the problem. In fact a 37 mm sphere at a depth .75m is beyond the detectability of BUD. If the seawater response were cancelled to 1 % of its value by the differencing scheme discussed below the target response rises well above the difference response for most of the useful time window of the transient. The transient responses for this configuration when both transmitter and receiver are on the surface of a conducting half space are also shown in Figure 1 for a range of ground resistivities. Cancelling the seawater response restores the sensitivity of MBUD to that of BUD over a typical 10 Ohm. ground.

The unique feature in the BUD system of measuring the differences of receivers placed symmetrically on either side of the transmitters cancels the seawater response because the induced currents in the seawater are also symmetric with respect to the transmitters. If all the symmetric receivers are in a single horizontal plane parallel to the air-sea interface and to the sea bottom then the layered response of these interfaces is also cancelled in the differences. The UXO target closer to one of the receivers then stands out against a null field background with essentially the same response as it would have in the land-based system. MBUD has capitalized on this unique feature of the BUD system and appears to have the same discrimination abilities as BUD for objects larger than 60 mm on or beneath the ocean bottom.

The differencing concept is illustrated for the simple two-receiver system shown below.

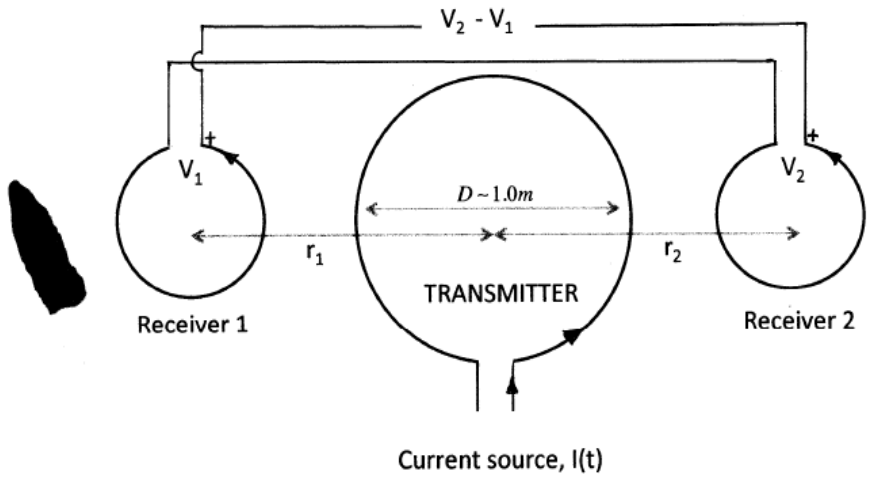

Figure 2

For symmetrically placed identical induction receiver coils, wired in opposition, the output voltage, V_2-V_1, is zero during the primary field pulse in free-space, *and at all times in a uniform conducting medium or in the vicinity of parallel plane interfaces in the plane of the transmitter and receiver.* When a conducting object is near one of the receivers the output is non-zero and is proportional to the difference of the object's secondary field at the two receivers.

This report details the steps leading up to the marine tests of the prototype MBUD system. It is organized in sections referenced to the Tasks in the proposal.

Task 1. Optimization of Transmitter-Receiver configuration and design of a receiver sensor.

a) Time-domain magnetic and electric fields from an arbitrary loop in a conductive medium

The presence of highly conducting seawater introduces three phenomena that are not noticed when the conducting target is embedded in the relatively modest conductivity of typical land soils. The first, as already mentioned, is the fact that there is a large transient response from the conducting seawater itself. The second is there is some attenuation of the primary field at the target and further attenuation of the target signal back to the receiver. In the frequency domain this is manifested as a change in amplitude in phases of the primary field as it reaches the target and a further change in amplitude and phase as it returns to the receiver. In the transient this can cause a reversal in sign of the transient, called a cross-over, at some, usually

early, time in the transient. Again this is not noticed in land-based systems because the soil conductivity is not high enough to introduce appreciable attenuation at the late times that are typically measured. Finally there is an electric dipole moment induced in a conducting target by the currents flowing in the conducting seawater. These currents are channeled into the good conductor and they produce magnetic and electric fields from the induced electric dipole. The induced electric dipole moments are in general orthogonal to the induced magnetic moments and the secondary magnetic fields they produce at a receiver can be in the same direction as common orthogonal to or opposite to the secondary fields from the magnetic dipole. The induced electric dipole depends very much on the surface condition of the target; for example an insulated steel ball would have no induced electric moment and would behave very much as it would in free space albeit with a slight attenuation caused by the seawater between the transmitter and receiver. For practical UXO systems the effects of the induced electric moment occurs at early times and are probably not seen in the window used for interpretation. Future systems might use very early time measurements to characterize additional surface properties of the object.
The numerical program for calculating the magnetic fields from an arbitrary loop source was rewritten to obtain the fields in a conducting medium. For this preliminary study for MBUD the induced electric dipole was not included. This code was then used to calculate the induced magnetic field at a spheroidal target, the induced magnetic moments, and the resulting transients at receiver locations. The results obtained in the first marine tests suggest that the induced electric dipole cannot be ignored and that the seawater effect on the transient must also be considered. A complete modeling code to include both these effects is to be included in Phase II of this project.

b) Optimum transmitter receiver configuration

Several transmitter receiver geometries were investigated using the modified code described above. Torquil Smith designed the BUD system by developing algorithms using these forward modeling codes to invert for optimum receiver positions. One of the configurations investigated for BUD used three orthogonal transmitters with three component receivers arranged on the base plane of the transmitter ‘cube’. This configuration was reanalyzed and the design represented by Figure 3 was selected for MBUD.

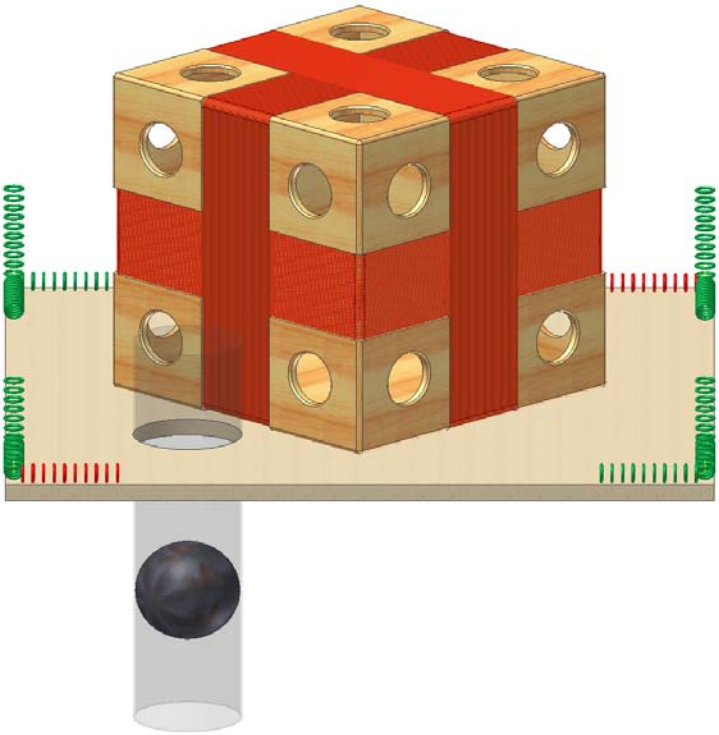

Figure 3

A plan view of this configuration is shown in Figure 4.

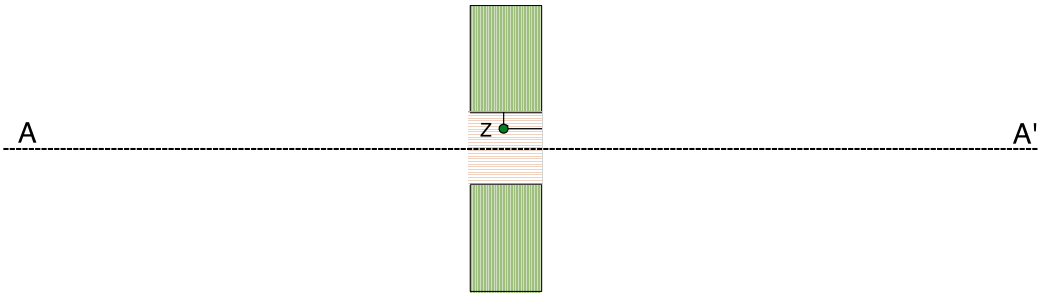

Figure 4

In the MBUD configuration four 3-component receivers are placed on horizontal plane beneath a three-component transmitter cube. Diametrically symmetric receivers see the same response from the seawater *and from the horizontal air-sea interface* and both responses are cancelled in the difference. In some cases the receiver outputs of a particular pair for one transmitter coil are of the same sign and must be differenced by the acquisition for another coil they are of opposite sign and must be summed. Figures 3 and 4 also show the test arrangement for positioning the 152.4 mm steel ball used as a test object.

In principle, data from the system may be inverted to estimate object position, and object polarizabilities as a function of time. The inversion code is now running for the MBUD configuration but has not yet been converted to include the effects of seawater on the computed responses. In its current form it is used give an idea of what size parameter uncertainties to expect due to residual seawater effects left in a set of data. In inverting data from a system, background fields from the response of seawater are expected to be the limiting factor in inversion for object parameters. The effective of background fields are reduced in two ways. Summing outputs from

diagonal pairs of horizontal component receivers cancels seawater responses for the horizontal magnetic field transmitter responses; differencing them cancels seawater response for the vertical magnetic field transmitter, and the opposite summing or differencing cancels seawater responses for the vertical component receivers. The other, non-cancelling, sums or differences of outputs of diagonal pairs of receivers can be reduced by differencing them with respect to reference measurements. Between the two we expect to be able to reduce the seawater response by a factor of 1/20 for non-cancelling receiver pair sums/differences and by a factor of 1/50 for cancelling receiver pair sums/differences. These figures were used as prospective errors in weighting synthetic data for inversion to evaluate system performance. Synthetic data sets were created for a series of 150 mm steel spheres centered 30cm below the device bottom plane along a line from system center through a point below one of the receivers (along the dashed line of Figure 4). Noise at the scale of the anticipated residual seawater response was added to the data, and the data inverted for object position and polarizability using the method of the method of Smith and Morrison (2004). Estimated errors in estimated sphere position are plotted in Figure 5 as a function of the sphere center position along the transect below the system. Estimated errors range from 8 mm error in horizontal position near the system center to 11 mm error in vertical position for a sphere below one of the system's receivers, and 12mm below the system center.

Est. Position Errors, 152.4 mm spheres at 30 cm Depth

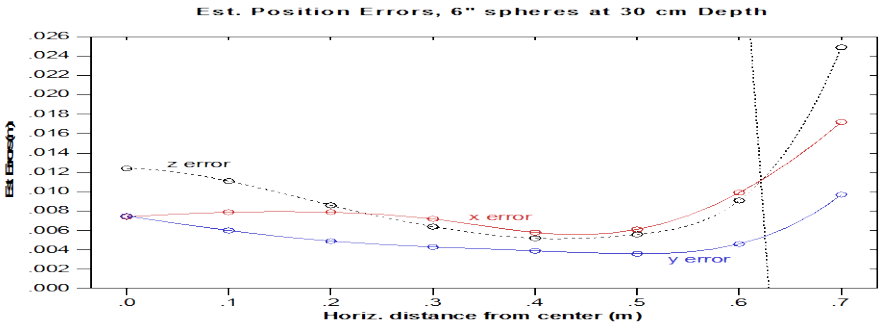

Figure 5

Estimated polarizabilities as a function of time are shown in Figure 6 for the results for a sounding over the sphere 30 cm from the device centerline. The plot shows that within anticipated scatter the three polarizabilities curves appear to overlay each other, as is characteristic of a sphere response.

152.4 mm Steel Sphere at 30 cm from the device centerline

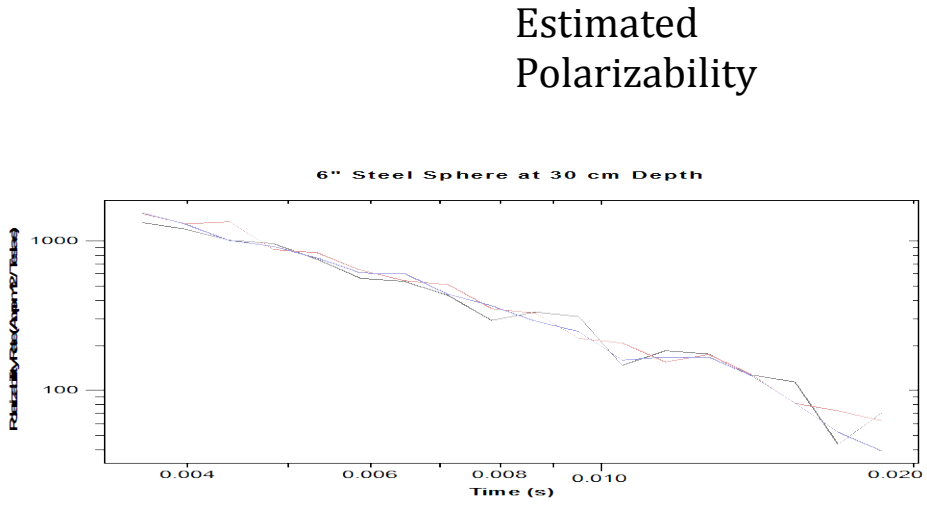

Figure 6

c) Size vs. depth of detection

This configuration was then used to simulate the response of the 152.4 mm steel ball as a function of depth at the location indicated in Figure 4. Examples of the response seen by particular pair of receivers for different depths of the target beneath the plane of the receivers are shown in Figures 7 and 8.

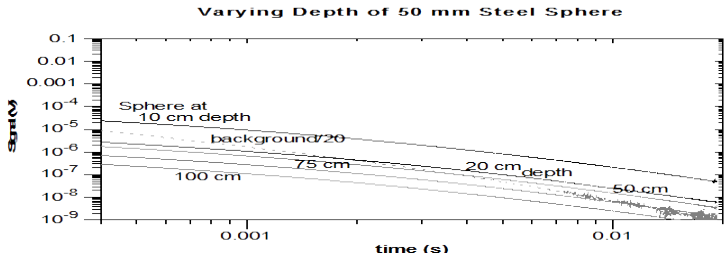

Figure 7

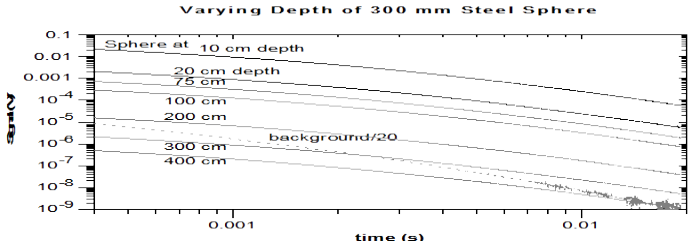

Figure 8

The dashed line in these plots shows the background or seawater response reduced by a factor of 20, i.e. a cancellation of 5%. A conservative estimate of the depth of detection can be made by determining the greatest depth at which the sphere response crosses the canceled background response within the time window where the response is above the noise level of the system (here taken to be 10^{-9} V). Thus, in Figure 6 the 50 mm steel sphere crosses the background response at about 0.8 m depth. From Figure 7 a 300 mm sphere could just be seen at a depth of 4 m. From a suite of such plots the size-depth plot of Figure 9 was projected. Graph is in meters

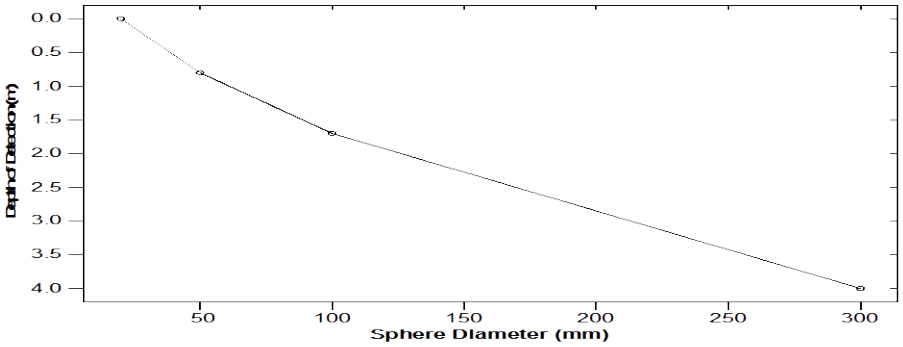

Figure 9

Figure 10 below is a similar size-depth plot that was constructed for the BUD system using similar assumptions but for 3.5:1 aspect ratio spheroids. The scales in Figures 9 and 10 are different, reflecting the expected greater depth of detection for large objects with MBUD. Nevertheless it is clear that MBUD has greater projected depths of detection than BUD for objects larger than 50 mm. This is a result of using three component receivers all in the base plane of the system and all as close as possible to the target, the greater separation of the receivers in MBUD, the higher moment of the MBUD transmitters and the higher gradients of the primary field in MBUD due to the more compact or dipole-like configuration of the transmitter coils.

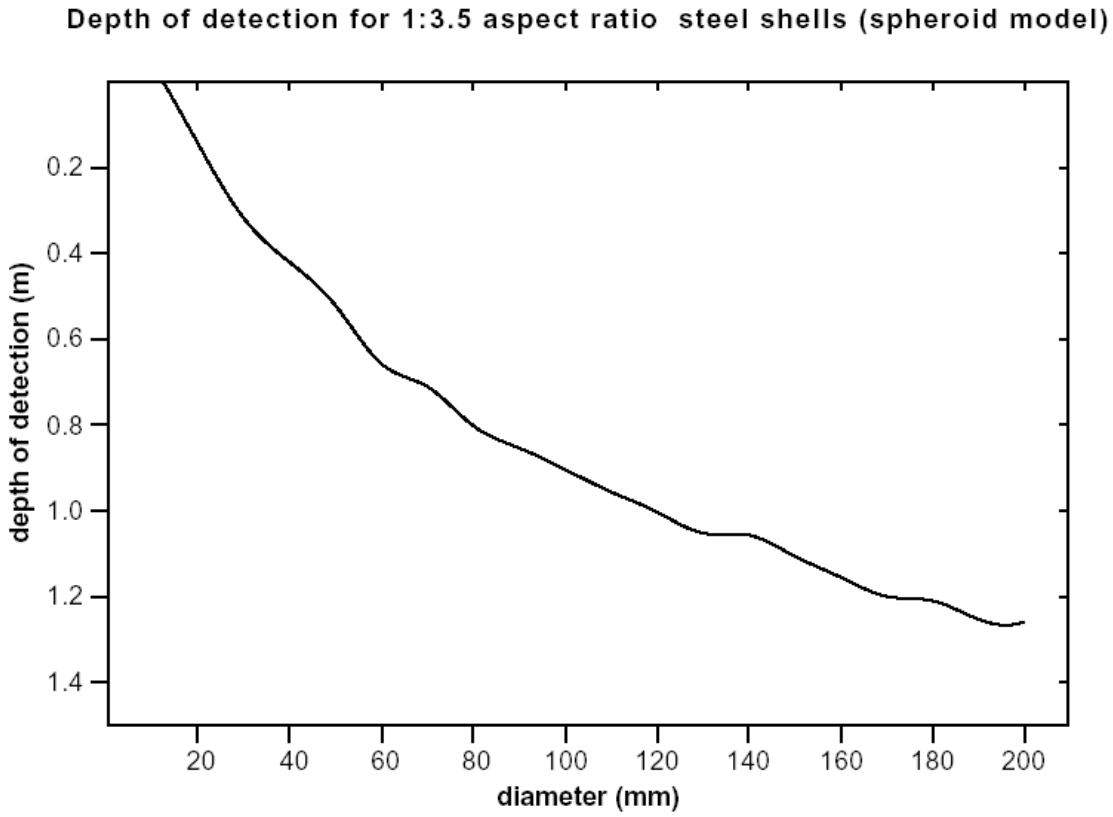

Figure 10

d) The effect of pulse width on the transient response

The effect of the half-sine pulse width on the amplitude of the target response and the seawater response is plotted in Figure 11. This plot was constructed by choosing the difference response for a particular pair of receivers, NA and SA in Figure 4, for the 152.4 mm steel sphere at 0.572 m depth for values of the pulse length between 1 and 7 msec. (the pulse width was 1.0 msec. for BUD). Of course the seawater response also changes with pulse length and this background response is plotted assuming that the differencing cancellation is good only to 5%.

The first thing to note is that at early time in the transient, say for less than 1.0 msec. the transient amplitude diminishes with increasing pulse length whereas at late times the transient amplitude *increases* with pulse length. This is important because an increase in amplitude at times where the amplitude is approaching the noise level of the system is advantageous. The same effect is noted in the seawater or background response. However note that the crossover point where the sphere response rises above the background response moves to earlier time as the pulse length increases. From Figure 11 it is seen that the crossover time for the 0.6 msec.

pulse is at about 1.0 msec. while for a 5.0 msec. pulse it is at about 0.2 msec. Lengthening the pulse therefore not only raises the response to background ratio at late time but it also increases the time window where the target response exceeds the background. The effect may appear subtle in the log plot but at a time of 10.0 msec. the target response for a 5.0 msec. pulse is *three* times the response for the 1.0 msec. pulse.

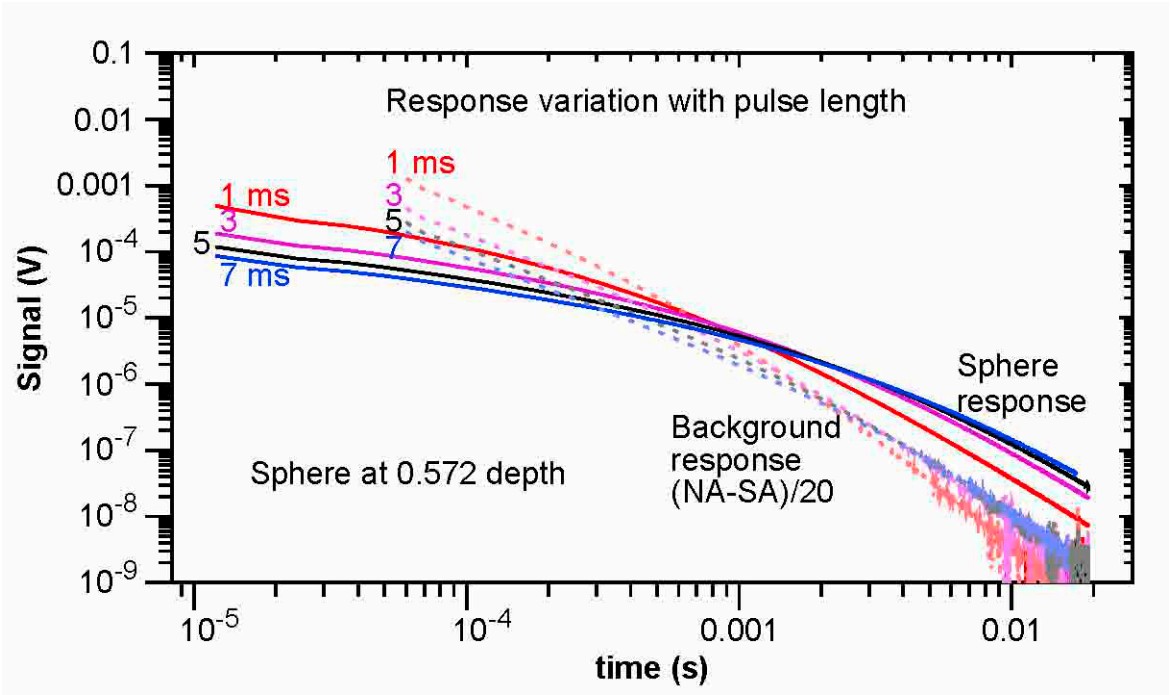

Figure 11

Based on this analysis the MBUD system was designed to have a 5.0 msec. pulse length. It will be seen in the section below on the design of the pulse forming circuit that this has the added advantage of reducing the demands on the switches in that circuit.

e) The effect of the air-sea interface on the transient responses

The air-sea interface affects the transient response as seen in Figure 12. For simplicity in demonstrating the effect the configuration of a co-located horizontal loop system was simulated for a step function current turn-off. The transient grows in amplitude by a factor of almost three as the system goes from the air-sea interface to great depth. At very early times the fields do not sense the interface but at the times typically used in MBUD the depth dependence is quite strong. For example, at 1.0 msec. the transient grows by about 40 % as the depth increases from 1.0 to 3.0 meters. Left unaccounted for this effect biases the transient and would have a major impact on the depth and polarizability estimates. Presumably a correction could be made by measuring the depth but as stated above the effect is cancelled in the difference scheme used in MBUD.

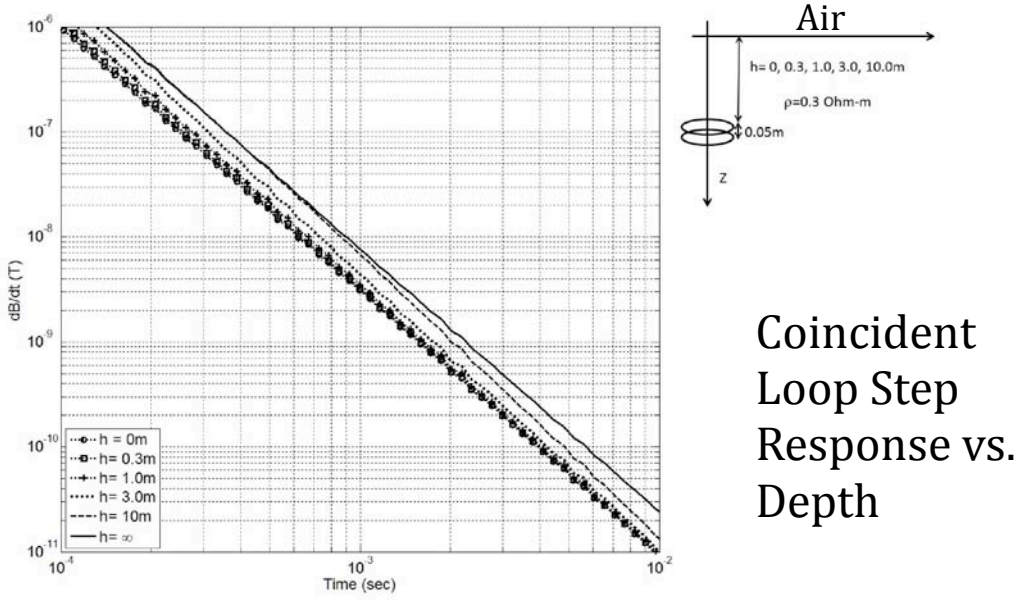

Figure 12

Another subtask was added to Task 1 as the project progressed. A concern arose after submitting the proposal that there might be a problem driving the desired current pulse in a transmitting loop *immersed in seawater*. Theoretically the inductance and resistance of such a loop are changed by the back emf's created by the induced currents (reducing the inductance) and by the resistive losses of the induced current (increasing the resistance). If either of these effects were appreciable they would have to be included in the pulse design circuitry. An approximate analysis simply using the induction number of a finite loop in a conducting medium suggested that the effect was small but perhaps borderline.

To settle the issue a small loop of approximately the size, resistance and inductance of the planned MBUD transmitter was made and submerged in seawater. The measured inductance dropped by only 1.5% at 10 kHz and the change in resistance was too small to be measured. It can be concluded that the loading of the transmitter coil by seawater is of no impact in the pulser design.

Task 2. Fabrication and testing of new receiver sensors in difference mode.

The MBUD prototype uses ferrite cored feedback coils developed by Morrison et al. 1984 and first implemented commercially by Ugo Conti at ElectroMagnetic Instruments, Inc. The coil and its associated amplifier is feedback enabled; the advantage is that with very little feedback the response is very stable through the self resonance which leads to much better performance in the difference mode of operation. Furthermore the coil and its amplifier have lower intrinsic noise level than the critically damped receivers used previously. A prototype of such a coil for possible use in the handheld BUD system was described in detail in a recent LBL/SERDP report: Morrison et al. 2011.

A potential problem that was identified in the proposal for the current project was that the sensor would saturate when exposed to very large fields directly from the transmitter during the current pulse. It was anticipated that a means would have to be found to protect the ferrite cored coil and its amplifier during the pulse. In fact the sensors made for MBUD did not saturate for the pulses generated in the prototype provided that the first stage gain was kept to 2.4. This meant that the coil amplifier combination could measure the transient directly and that the differences could be taken in a second stage where more gain could be added after differencing to bring the signal level up to the input requirements of the data acquisition system.

These sensors are very compact and have the same sensitivity as the air-cored coils used in BUD. Again, without the weight limitations of BUD, these coils have much higher sensitivity than any receivers previously used for UXO detection and discrimination. In addition the cylindrical shape lends itself to efficient mounting in a rigid tubular style frame.

The MBUD magnetic field sensor.

All induction coils magnetic field sensors have the equivalent circuit representation shown below, Figure 13

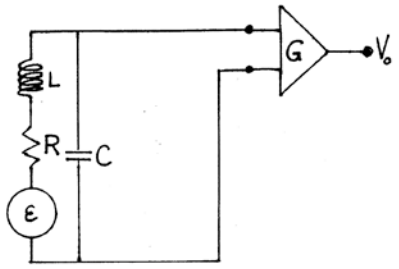

Figure 13

The emf, ε, is caused by the changing magnetic field threading the coil, dB_0/dt. It is a voltage source in series with the coil inductance, L, and the coil resistance, R. In practice it is observed that the multi-turn coil also has a distributed capacitance C due to the intra-wire capacitance of the turns in the coil. The effect of the capacitance is to provide a load impedance for the coil so that as the frequency increases current flows through the capacitance and the observed voltage on the terminals decreases. The circuit is also becomes a resonant circuit.

The frequency response of this circuit has a well-known form:

$$\frac{V_0(\omega)}{B_0(\omega)} = \frac{i\omega\omega_0^2 F}{\omega_0^2 + 2\alpha i\omega\omega_0 - \omega^2}$$

where F is a physical property of the ferrite coil/ amplifier combination equal to $G\mu_{eff}NA$ and N is the number of turns, A the cross sectional area of the coil, μ_{eff} is the effective magnetic permeability of the ferrite core and G is the gain of the amplifier.

In this expression the resonant frequency is $\omega_0, = \frac{1}{\sqrt{LC}}$ and the response parameter is related to the Q of the circuit via: $\alpha = \frac{R}{2\omega_0 L} = \frac{1}{2Q}$.

A typical frequency amplitude response is plotted in Figure 14.

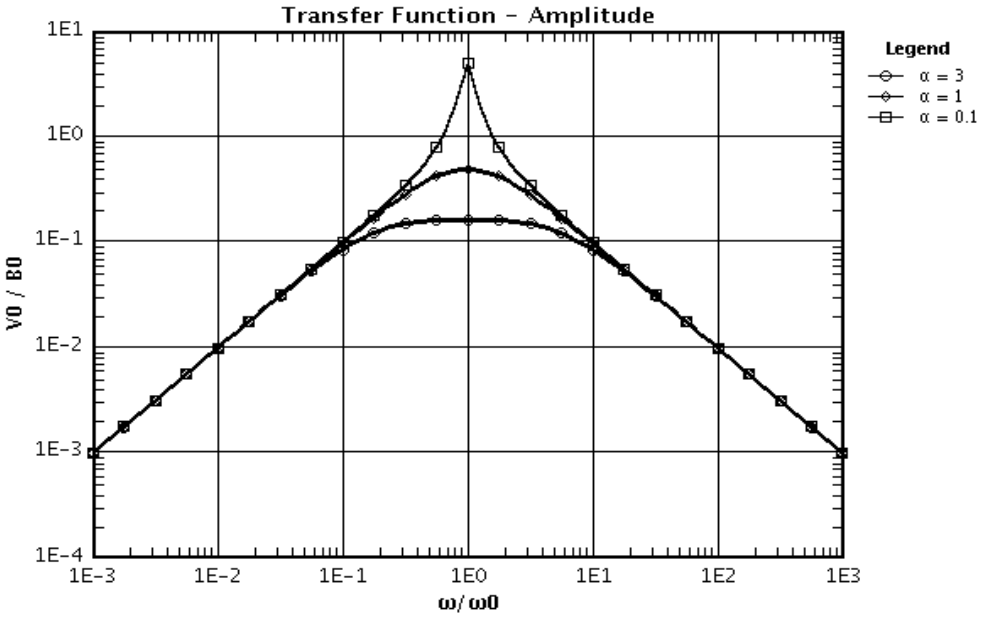

Figure 14

The significance of α is best understood by considering the transient response of the circuit for a step function turn off of the magnetic field, Figure 15.

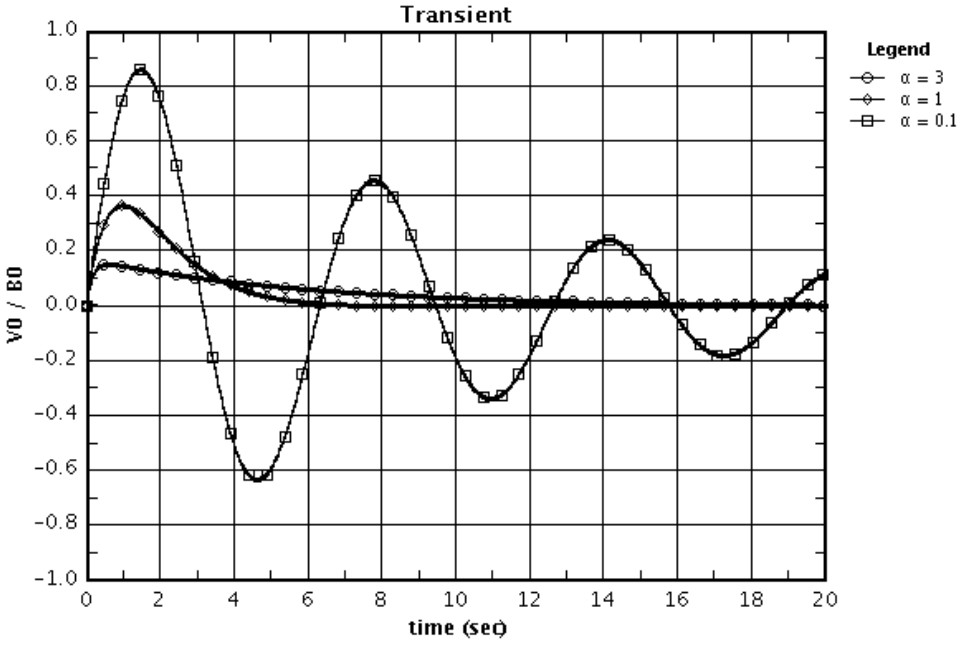

Figure 15

When α is less than 1.0 the circuit is *under damped* and the output has a damped oscillation or 'ring' which is obviously not desirable because it would obscure the desired transient signal from the conductive target. For α greater than 1.0 the circuit is *over damped* and the output amplitude is reduced and it persists with a slow decay in time, again obscuring the desired transient. For α = 1.0 the circuit is *critically damped*: it has the fastest possible decay without ever crossing zero. This is the optimal circuit for recovering target transients and is a basic design objective for BUD and MBUD.

In general it is not possible to make the coil resistance and inductance values equal to the value needed for critical damping. Practical considerations on weight, size, and number of turns usually set the wire diameter and length and hence the resistance and inductance. The effective resistance can be set through the addition of an external damping resistance, as shown in Figure 16.

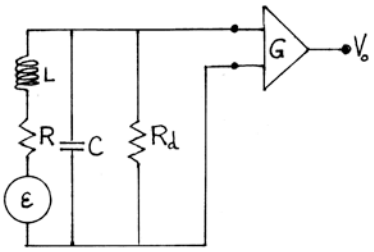

Figure 16

With some analysis the response of this circuit reduces to the same form as the circuit in Figure 15 with a modified definition of α *and modified resonant frequency.*

$$\frac{V_0(\omega)}{B_0(\omega)} = \frac{R'}{R} \cdot \frac{i\omega\omega_1^2 F}{\omega_1^2 + 2\alpha i\omega\omega_1 - \omega^2},$$

where, now $R' = \dfrac{RR_d}{R+R_d}$, $\omega_1 = \omega_0\sqrt{\dfrac{R}{R'}} = \omega_0\sqrt{\dfrac{R+R_d}{R_d}}$ and $\alpha = \dfrac{\omega_1}{2}\left(\dfrac{L}{R+R_d} + R'C\right)$.

As before critical damping is now achieved by choosing R_d to make α = 1.0. The analytical expression for R_d is complicated but it becomes evident when analyzing practical coils that R_d must much larger than R and so $\omega_1 \approx \omega_0$ and $\omega_0 L > R$ and so finally the expression for R_d simplifies to:

$$R_d \approx \frac{\omega_0 L}{2}.$$

A problem with the BUD circuit was that although it was fairly easy to achieve critical damping with the adjustable external resistor, the very small change in resonant frequency made it difficult to tune two resonant circuits to achieve accurate analog cancellation in difference mode. As the components of the sensing loop changed slightly in response to temperature variations the corresponding differences of the transient signal became a significant source of noise.

Electromagnetic geophysicists encountered similar problems in the 1980's in trying to make very accurate phase measurement of frequency domain systems. An alternate way to control the bandwidth of the induction sensor and to achieve critical damping without changing the resonant frequency and to achieve high phase stability is to implement the negative feedback scheme as shown in the circuit of Figure 17 below.

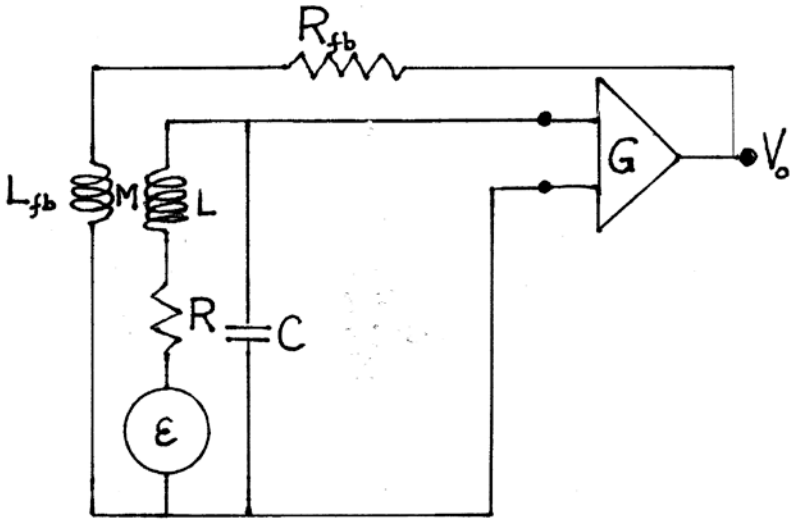

Figure 17

In this circuit a small current is driven back through a feedback resistor, R_{fb}, to a coil of inductance L_{fb} that is coupled to the main coil with a mutual inductance M.

With the correct sign for M this couples an emf, ε_{fb}, into the primary circuit in opposition to the emf induced by the changing external field. The voltage induced in the receiver coil is simply $\varepsilon_{fb} = -\frac{M}{R}\frac{\partial V_0}{\partial t}$ and the voltage induced by the changing

external field is, as before, $\varepsilon(\omega) = -i\omega\mu_{eff} NAB_0(\omega)$. The current, I, that flows in the RLC circuit is $\frac{\varepsilon + \varepsilon_{fb}}{Z}$ where Z is the series impedance of R, L and C given by

$$Z = R + i\omega L + \frac{1}{i\omega C}$$

Again, after a bit of analysis this reduces to the familiar form for the response:

$$\frac{V_0(\omega)}{B_0(\omega)} = \frac{i\omega\omega_0^2 F}{\omega_0^2 + 2\alpha i\omega\omega_0 - \omega^2}$$

where, now, $\alpha = \frac{R}{2\omega_0 L} + \frac{\omega_0 MG}{2R_{fb}}$.

So if α is too small because R may be too small, it can be increased arbitrarily by adding the term $\frac{\omega_0 MG}{2R_{fb}}$. There is some flexibility in choosing M, G and R_{fb} so it is easy in practice to achieve any desired value of α and in particular to achieve critical damping $(\alpha = 1.0)$. The added importance of this becomes evident when we find that $\frac{\omega_0 MG}{2R_{fb}}$ is usually much greater than $\frac{R}{2\omega_0 L}$ and so instabilities in R or L become insignificant and the stability of the critically damped response depends mostly on MG/R_{fb} all of the terms of which are easily held constant. When $\frac{\omega_0 MG}{2R_{fb}}$ is greater than $\frac{R}{2\omega_0 L}$ the criteria for selecting the feedback resistor simplifies to:

$R_{fb} = \frac{\omega_0 MG}{2}$.

The mutual inductance is given by: $M = k\sqrt{L\,L_{fb}}$ and because the feedback coil is co-wound on the main coil *k* can be assumed to be one.

This is the circuit used in the new MBUD system.

The new MBUD coil is shown in the photo below and its dimensions and circuit properties are tabulated below the photo.

MBUD Ferrite Cored Feedback Induction Coil Sensor

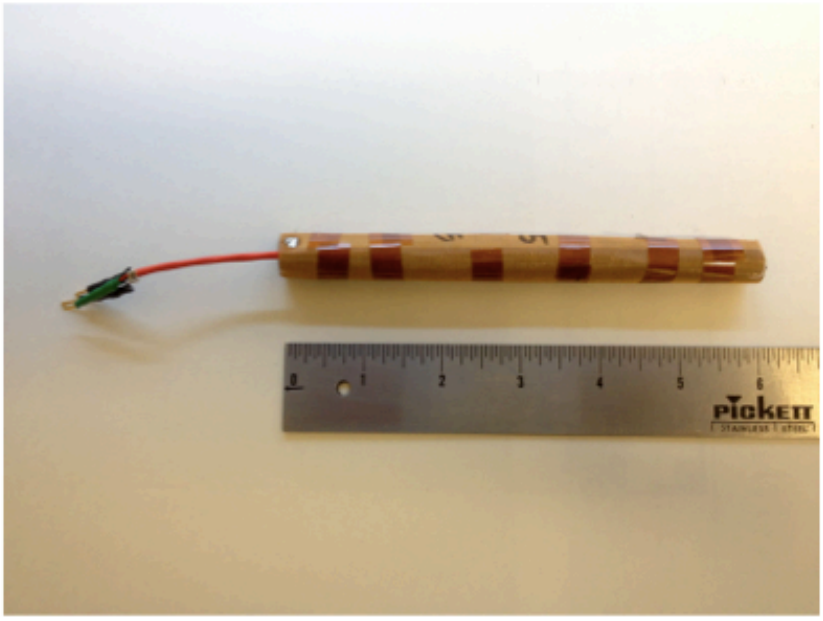

Length: 152.4 mm (6 inches) Number of turns: 775 Core diameter: 10 mm
Core effective permeability: 80
Inductance: 51 mH Capacitance: 200 pF Resistance: 10 Ohms
Feedback resistance: 2000 Ohms Feedback mutual inductance: 4.1 mH

Figure 18a

The circuit schematic used for the MBUD sensor is shown in Figure 18b. This circuit provides adjustments for gain, feedback resistor and tuning capacitors allowing multiple means for matching coils used in difference mode.

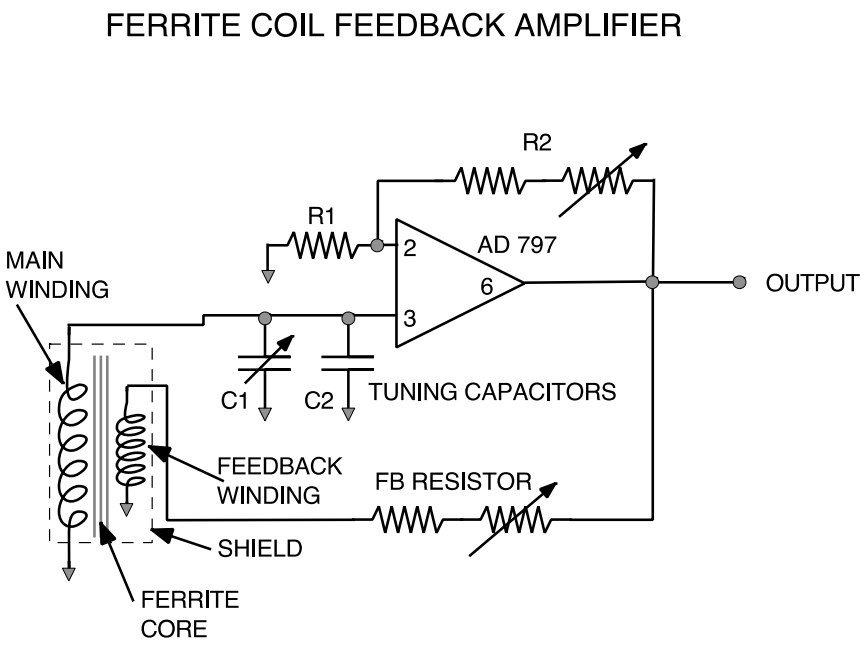

Figure 18b

The gain for the associated amplifier was chosen to be low, 2.4, to prevent saturation during the large primary field pulse. The gain and coil parameters were used in the above analytic expression for the feedback coil circuit and the following response in Volts per Tesla was calculated (Figure 19). The α value for these parameters is about 0.8 so the coil should be slightly under damped: in fact the actual coil is critically damped. Errors in the calculation of the mutual inductance used in the response formula probably account for this small discrepancy between predicted and measured values.

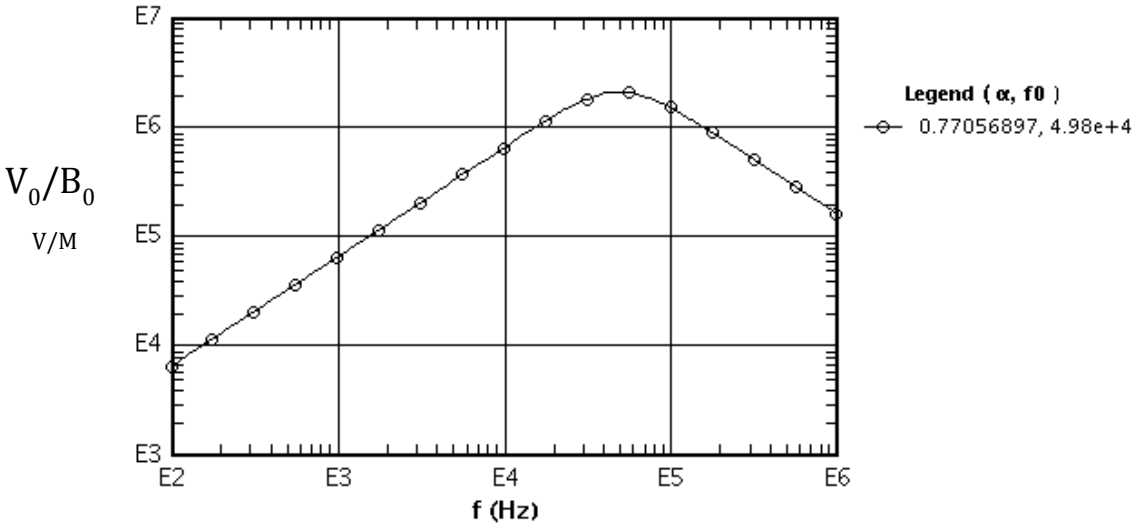

Figure 19

The measured response of the MBUD sensor is plotted in Figure 20. Transient responses showed proper critically damped response.

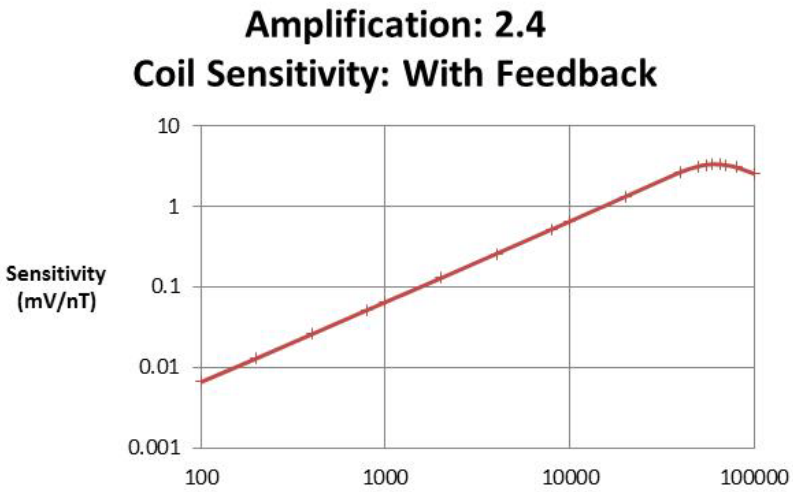

Figure 20

The peak response at the resonance frequency is 3.3 mV/nT whereas the predicted response at resonance for the circuit simulation, Figure 19, is 2.2 mV/nT (2.2×10^6 V/T). Again the small discrepancy in value is probably due to an incorrect value for the mutual inductance used in the numerical calculation.

The analytic expressions for the response of the feedback circuit can be used for computing the expected noise level of the sensor for the specified values of the circuit parameters and for any given amplifier. This process revealed that in working with a fairly high inductance source impedance the choice of amplifier is quite critical especially the levels of input current noise. Figure 21 shows the calculated noise for the new MBUD sensor along with the noise for the BUD system that used a different amplifier

Run 1: 152.4 mm ferrite cored feedback coil

Run 2: 127 mm diam. Air cored coil from BUD

x = measured noise

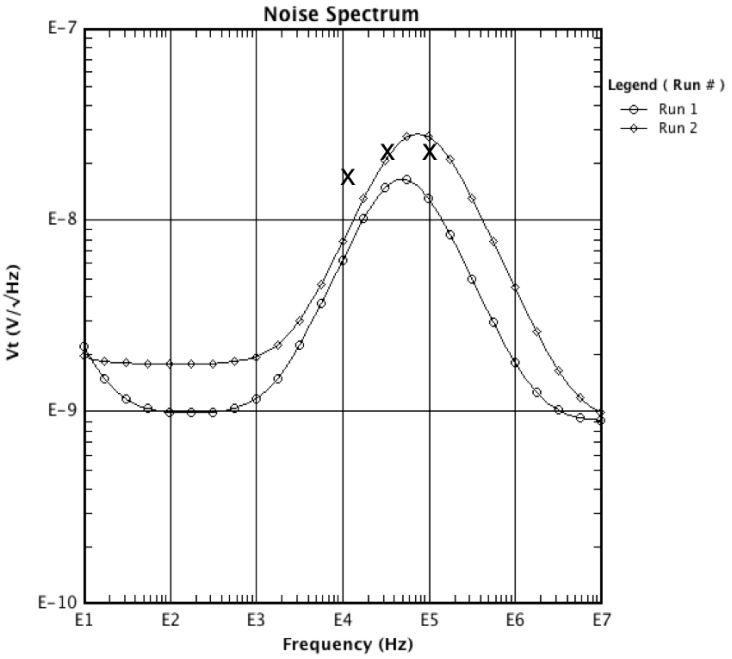

Figure 21

Crude measured values of the noise using measured values of spectrum and coherence for two parallel sensors are also plotted on Figure 21. These measurements were difficult to make in a noisy lab but clearly show that the resulting MBUD sensors have the predicted low noise.

The new MBUD sensors have about half the noise of the BUD sensors: this is not a small improvement: in practice it translates into a signal to noise gain of two, equivalent to doubling the source moment. Since the MBUD moment is larger than that of BUD the performance of MBUD should be a factor of at least two better than BUD.

After several fabrication and testing experiments, the first four sensors that were rigorously tested behaved so well that the decision was made to make enough for the final MBUD design. Having decided that the optimum array involved four three-component sensors (see Figures 3 and 4), a set of twelve that were closely matched in properties were made.

The coil were sealed in cylindrical plastic tubes and mounted in machined plastic blocks with a hollowed-out core that houses the three individual amplifiers for each of the three coils. The resulting three-sensor receiver ‘cube’ is shown in Figure 22.

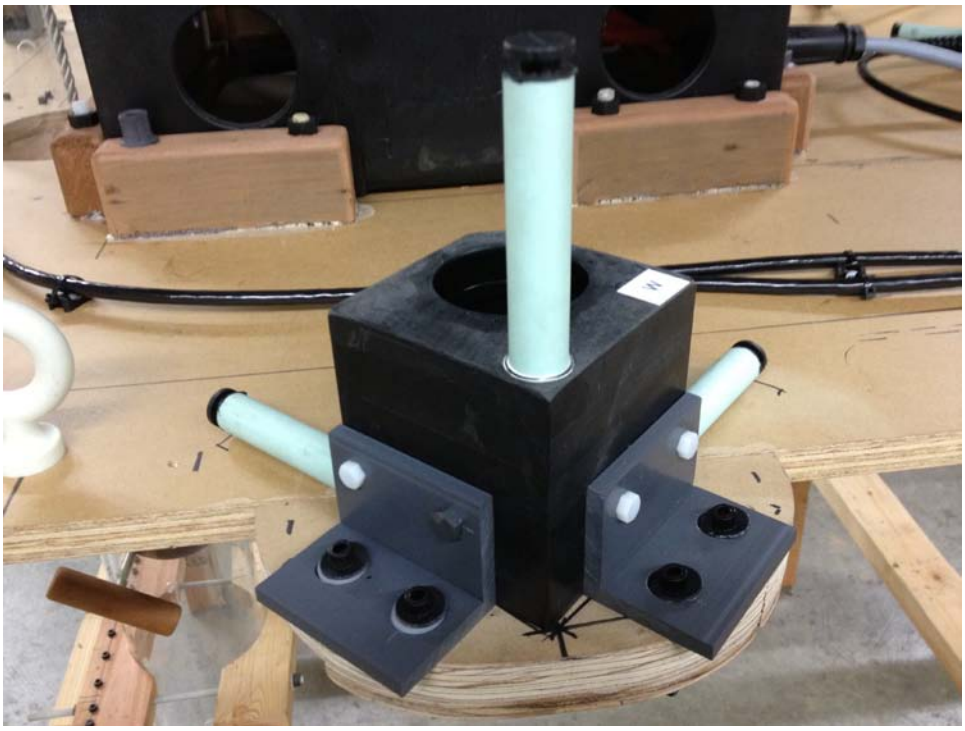

Figure 22

The individual coil/amplifiers are each connected to the central acquisition unit where appropriate sensors are combined in pairs forming the inputs to differencing amplifiers with more gain to bring the difference signals up to the required input level of the analog to digital converters (ADC). It is important to note that this scheme removes the spurious coupling issues that plagued the BUD system wherein the coils were wired in opposition and then fed to the amplifiers of the ADC over long wires snaking across the transmitter coils. In MBUD the initial gain at the coil provides a low impedance source and relatively high level signal that is relatively immune to spurious coupling on the connecting cables. The new configuration is only possible because in MBUD the amplifiers can sustain higher voltages before saturation, the sensor/amplifiers are relatively farther from the transmitter (in BUD the flat air-core sensors were mounted *on* the transmitter frame and some were maximally coupled to one or more of the transmitter windings) and the orientation and location of the sensor ‘cubes’ could be adjusted to minimize the direct primary field coupling.

Task 3. Redesign of system controller, data acquisition and fabrication of high-power pulser.

All these items were taken from the LBL BUD system. Descriptions of the individual components have changed very little from the basic technical report by Beche et al. 2005.

The FPGA provides the sequence of control pulses that turn on the pulser for each half-sine pulse. It distributes the control pulses to drive each of the orthogonal transmitters in a preplanned sequence and for a preplanned number of pulses and repetition rate. It required very little reprogramming to accommodate the pulse sequence and duration for MBUD. Similarly the data acquisition board was used directly (it is also controlled by the FPGA to achieve synchronization of the digital stacking of the transients with the transmitter pulses.).

The pulser design for MBUD was a modified version of the BUD design. The MBUD coils have a different inductance than BUD and the pulse length is 5 msec. rather than 1.0 msec. necessitating different capacitors. Because of higher design current pulses the SCR switches also had to be different.

The MBUD pulser can drive three orthogonal transmitting coils (X, Y, and Z axis) at a single pulse width. The performance specifications are shown in Table 1.

Table 1: MBUD Pulser Requirements.

Pulse Width (ms)	5
Frequency (Hz)	12.5
Peak Current (A)	200

The pulser is a parallel matrix of four half-bridge circuits which can switch between three orthogonal transmitting coils (Figure 23). The high-side switches are inverter SCR's and low-side switches are phase control SCR's that are driven by custom gate drivers with the required voltage isolation.

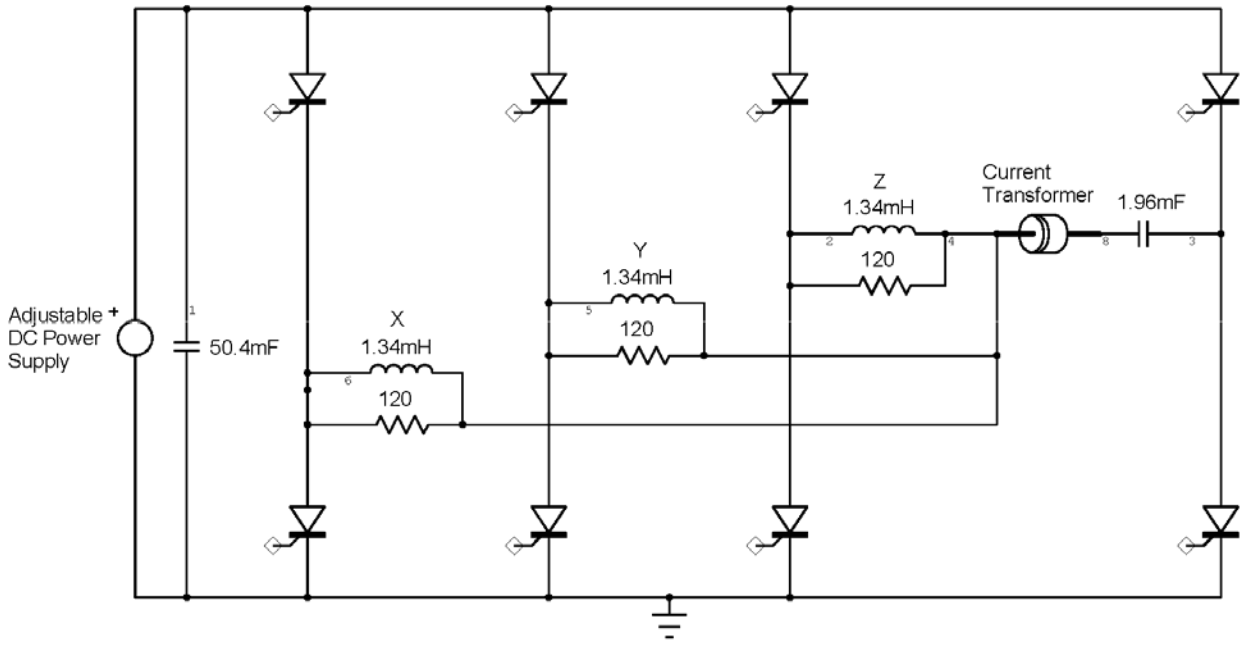

Figure 23: Simplified Pulser Schematic

Table 2: Major Components

Inverter SCR's	International Rectifier
Phase Control SCR's	Semikron SKKT106/16E
Microcontroller	Arduino Uno R3
Power Supply Capacitors	Cornell Dubilier CGS422U075R4C
Main Capacitors	Cornell Dubilier
Current Transformer	Pearson Electronics 101

For the prototype, fast turn-off inverter SCR's were chosen for the high-side switches to ensure that the current switches off within 100us of the zero-crossing for receiver and data acquisition considerations. Because there is always one high-side switch in series with the current, the low-side switches can be slower phase control SCR's. The high- side switches require isolated gate drivers because the gate drivers are referenced to the SCR cathodes that are floating. 1:1 pulse transformers provide this voltage isolation. The nominal gate drive to each SCR is 10V and 1A for 10-20us and is limited by the volt-seconds of the transformer core. For commonality, the same isolated gate drivers are used for the low-side switches even though these SCR's do not require isolation since their cathodes are at ground potential.

The low voltage triggers are generated by a commercially available microcontroller board that is programmed by a PC through a USB interface. Once

the microcontroller board is programmed, the role of the PC in changing the pulsing configuration can be substituted with a switch array attached to the microcontroller's I/O port. These triggers are inputs to the gate drivers which generate the required transmitter coil current pulse format.

Snubber circuits across the transmitter coils are required to suppress the amplitude of voltage transients generated when the current is shut off at the end of each half-sine pulse. Although the SCR's start to turn off at the zero crossing of the drive current, it takes some time for the SCR's to recover and so there is always some small amount of current flowing through the coil and circuit inductance at the time the SCR's open. This V=LdI/dt transient must be suppressed to protect the SCR's from a voltage spike which could overvoltage the devices. Note that these networks do increase the losses in the system and therefore increase the input power required, but this power is insignificant for systems with long current pulse widths compared to the transient pulse-widths. In this case, a 120 Ohm resistor was placed across each of the transmitter coils without a capacitor in series. To turn on, the SCR's need to see a moderate resistive load until the current has time to rise in the large inductive load. For the prototype system, the SCR's turn on when the power supply voltage is 30-32V.

The current through the transmitter coils is measured with a current transformer so that the appropriate power supply voltage can be determined. This diagnostic also has sufficient bandwidth to characterize transient behavior during the turn-off of the transmitter coil current. The conversion ratio is 100A/V when the current transformer is terminated into a high impedance ($\geq$ 1 Mohm) and 200A/V when terminated into 50 ohms.

In general, it is preferred to run an adjustable power supply in a voltage regulating mode after setting the current limit to just above what is required to meet the pulse format requirements. The current limit can then be used as a fault indicator and can also limit energy which can be deposited into a fault such as a short circuit. For a single output level, a DC battery could also be utilized as the primary power source.

For high voltage safety considerations, there are redundant bleed resistors across each of the capacitor banks to discharge any stored energy once the main power supply has been turned off. For the main capacitor bank, the discharge RC time constant is 61 seconds. The discharge RC time constant for the power supply capacitor bank is 55 seconds.

Because of current limitations of the available power supply during testing, the repetition rate was reduced to 12.5Hz to get the desired 200A transmitter coil

current (see Table 3). In general, it is the power supply voltage which determines the coil current and the power supply current which must support the average coil current. The Q of the resonant circuit determines the steady state capacitor charge voltage which is derived from the power supply voltage. To maintain this capacitor voltage, the power supply current must recharge the system fast enough so that the energy which is dissipated every cycle can be replaced or the capacitor voltage will fall to a lower level. From the measured values at 12.5Hz, the nominal pulse format from Table 1 will require ~1.1kW of input power.

Table 3: Prototype pulser test parameters.

Frequency	Coil Current	Coil Voltage	Capacitor Voltage	PS Voltage	PS Current	PS Power	Snubber details
12.5Hz	200A pk	200V pk	+/-165V	36.5V	12.5A	456W	R=120

Because the input voltage is fixed by a power supply or battery, if the losses in the system increase with temperature as the system is pulsing, the current in the transmitter coil will decrease. The characteristic impedance of the LC ringing circuit is ~0.8 ohms, so it is expected that increases in any resistive elements will not significantly reduce the output current amplitude, but adequate cooling of the pulser components and the transmitter coils will be required.

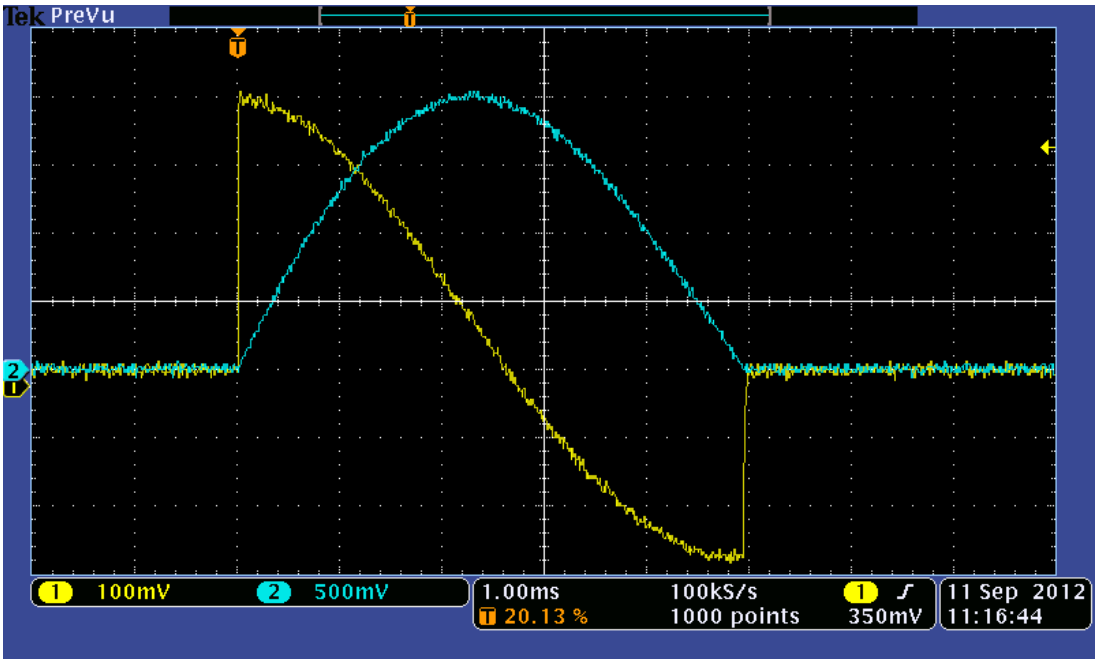

Figure 24: Typical transmitter coil voltage and current waveforms for the nominal pulse format at 200A. The yellow waveform is the coil voltage and is 50V/division. The blue waveform is the coil current and is 50A/division. The time scale is 1ms/division.

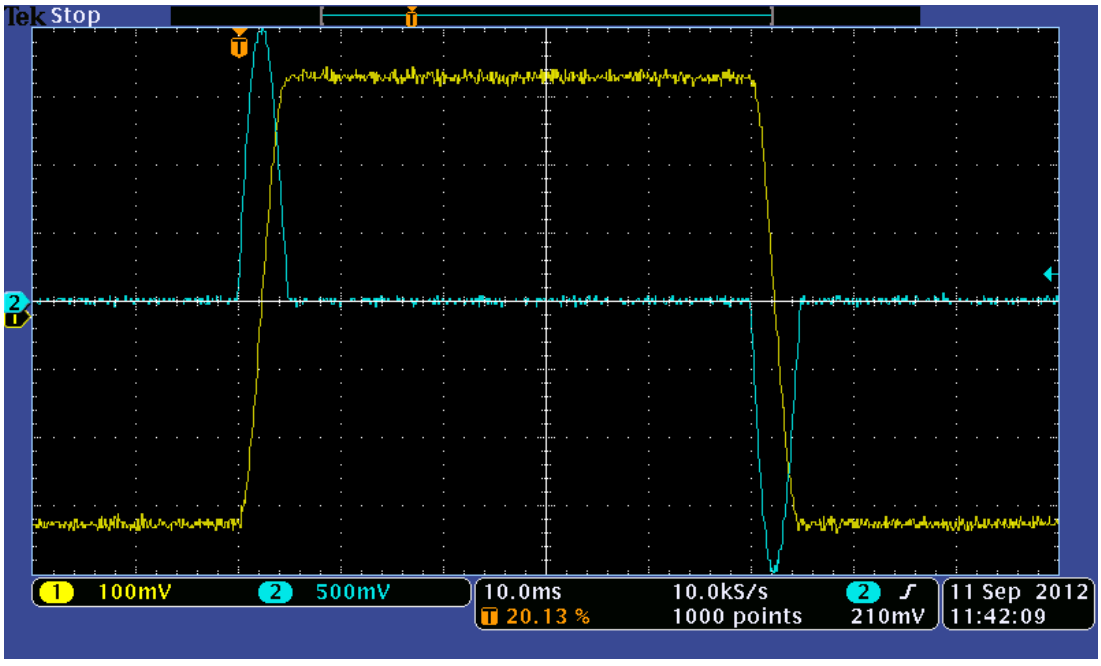

Figure 25: Typical main capacitor bank voltage and transmitter coil current waveforms for the test parameters shown in Table 3. The yellow waveform is the main capacitor bank voltage and is 50V/division. The blue waveform is the coil current and is 50A/division. The time scale is 10ms/division.

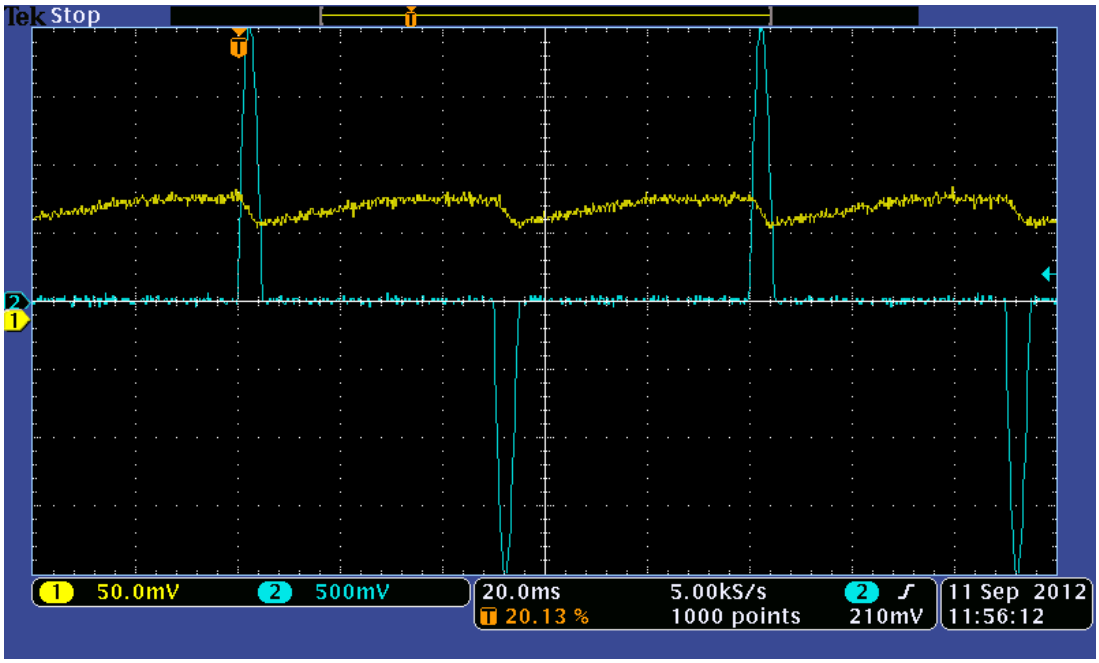

Figure 26: Typical power supply capacitor bank voltage and transmitter coil current waveforms for the test parameters shown in Table 3. The yellow waveform is the power supply capacitor bank voltage and is 25V/division. Note that there is a 7.5mV offset on this differential voltage probe so the reference position is the same for both channels. The power supply capacitor peak voltage is approximately 36.5V. The blue waveform is the coil current and is 50A/division. The time scale is 20ms/division.

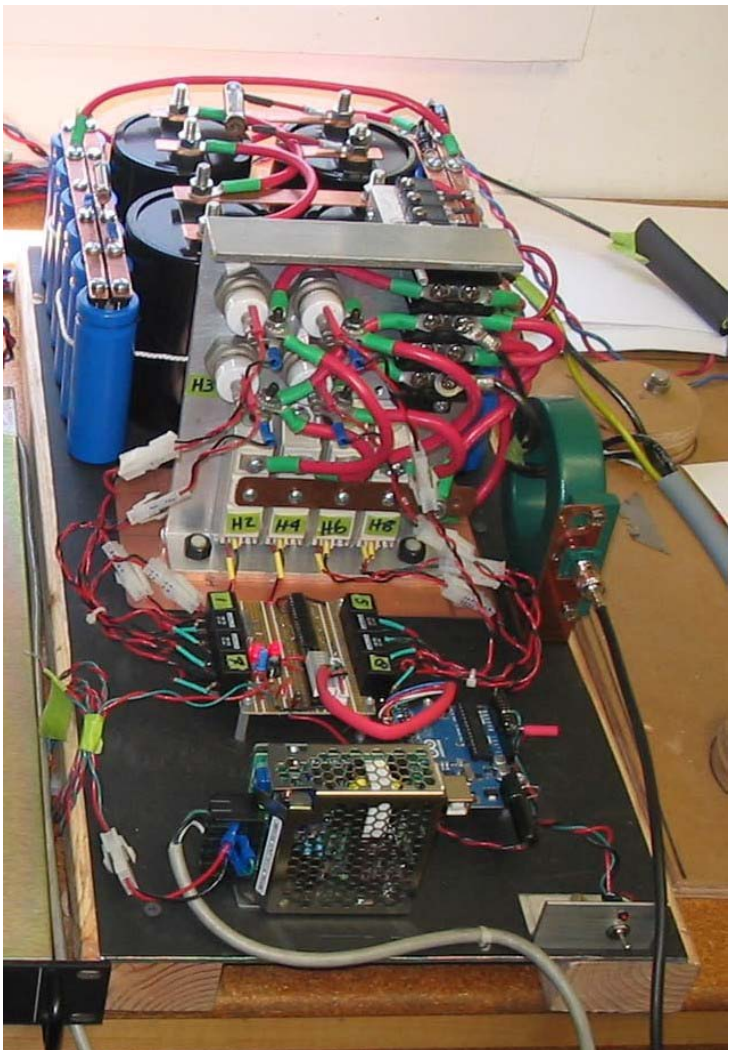

Figure 27: Picture of the prototype pulser.

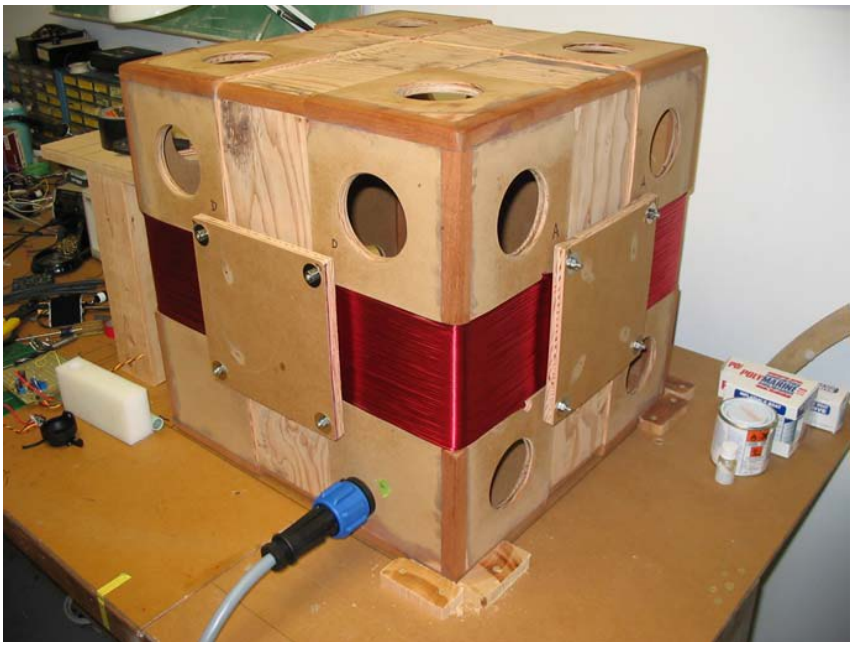

Figure 28: Picture of the test transmitter coil (one axis).

The pulser for the prototype MBUD is shown in its waterproof container in Figure 29.

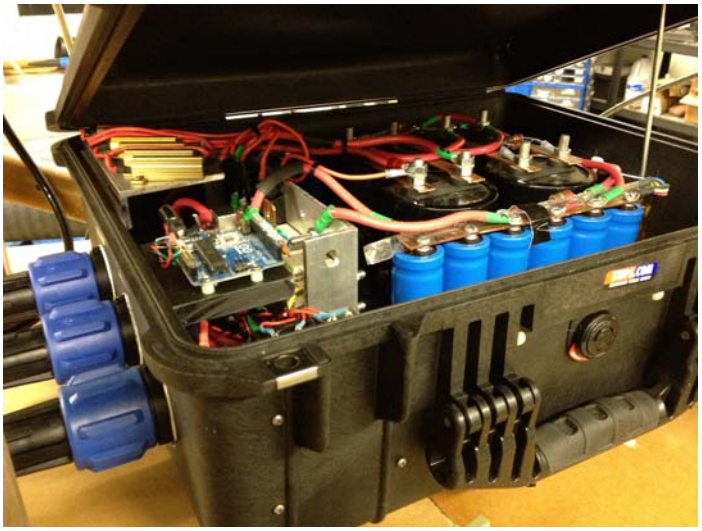

Figure 29

The prototype MBUD transmitter cube has 40 turns on each face as shown in Figure 3. The cube 50.8 cm on a side: the loop area is 0.258m^2. The peak moment is the product: Number of turns x Area x Peak current, so with a peak current of 200 A, the moment is 2060 Amp.Turns.M^2. The BUD transmitter had a moment of about 500 Amp.Turns.M^2.

Task 4. Tests of a marine prototype in shallow water.

MBUD Prototype System.

The proposed fourth task was the underwater testing of a prototype frame with a reduced set of paired receivers. In fact a full complement of four 3-axis sensors was used with all three transmitters activated in sequence.

A physical framework for the transmitters and receivers was designed following the dictates of the numerical optimization study discussed above. It was originally intended to only populate a few of the receiver positions with 4 to 8 pairs of single axis receivers to show the basic detectability of a UXO in the presence of seawater. Instead the full final MBUD configuration was tested with the intention of providing a complete data set ready to be used in the inversion process in Phase II to come. This approach led to the construction of a rigid frame, the mounting of the orthogonal transmitters, the testing of higher power pulser, and the wiring configuration of the full receiver set. The resulting prototype system has the final transmitter and receiver modules that can be used in the system to be tested in Phase II.

The transmitter cube and four three-sensor receiver cubes were mounted on the laminated waterproof platform as shown in Figures 29 and 30.

Figure 29

Figure 30

The receiver coils, and transmitter cube, are mounted as shown in the plan view schematic of Figure 4. The waterproof containers for the pulser unit and the data acquisition unit are mounted about 2 m away from the transmitter-receiver system. The control computer and pulser power supply were connected to the platform by a 10 m cable. The entire platform was mounted on legs with cement bucket feet so that when resting on the bottom the platform would be roughly one meter above the bottom. A plastic cylinder for accurately positioning the 152.4 mm steel test ball was mounted vertically between two of the receiver cubes as shown in Figure 29. The test steel ball was lowered to preset stops in this tube at depths beneath the platform.

The custom catamaran shown in Figure 31 was constructed to hold the platform assembly and to lower the assembly into the water.

Figure 31

The catamaran and MBUD system were mounted on a flatbed trailer, transported to the Richmond Marina, and launched from the boat launch ramp, Figure 32.

Figure 32

Once in the water the whole assembly was easily maneuvered into position alongside the dock and submerged in water, Figure 33 and 34.

Figure 33

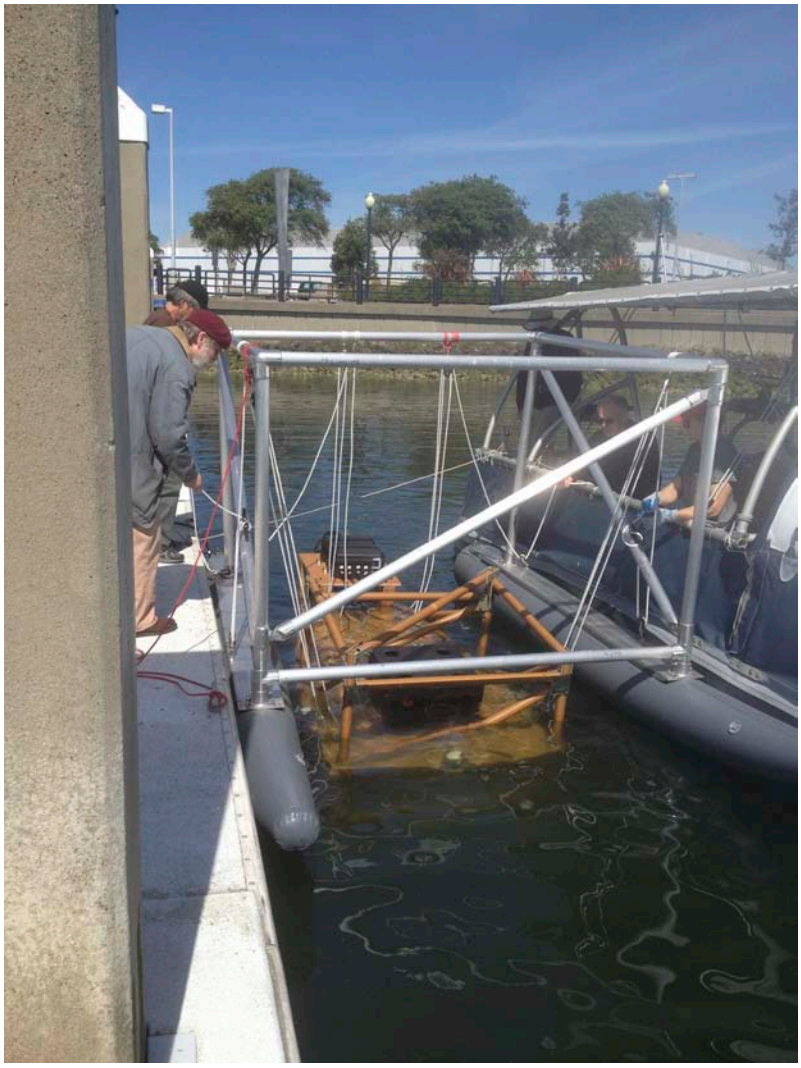

Figure 34

The water depth was about 5 m and the whole test was conducted in a short interval at high tide; the depth from the sea-air interface to the system did not vary appreciably during the test.

Background data were taken when the system first reached the bottom, data were taken for successive depths of the steel ball beneath the platform and background data were taken at the end of the tests with the steel ball removed. The steel ball was repositioned each time by a scuba diver.

MBUD Test Results

The prototype MBUD has a full complement of four 3-component receivers and three orthogonal transmitters. There are consequently a very large number of transmitter-receiver pairs that are essential for full data inversion for depth and polarizability of the target, but that too much for individual graphical representation. To demonstrate the results, a subset of the transmitter pairs has been selected and is discussed below. [The original proposal was to only build such a subset to demonstrate the properties of MBUD]. The full data set now available will accelerate the development of the inversion solutions to be implemented in Phase II.

Two horizontal sensors, NA and SA in Figure 4, were selected to show the transient responses for each of the three transmitters Bx, By and Bz. The 152.4 mm steel ball was positioned at successive depths of 0, 14, 29, 43, and 57 cm beneath the plane of the receivers. The background response is the transient response observed in the absence of the steel ball. The origin of the background response is not presently known: it includes imperfect cancellation of the response from the ground itself or from metallic objects/structures in the laboratory where the land tests were done. Similar residual transients were observed in BUD and other UXO systems. It may be that there are residual eddy currents flowing in the mass of copper in the transmitter after the current is shut off. In any event if the background is stable the transient with a target in place minus the background transient yields an accurate measure of the target transient itself. In the transient plots shown below the background response has been subtracted. The stability of the background transient is measured by differencing two background transients and this is shown in the plots as the 'noise level'. The background transients themselves also displayed noise due to pick-up of local electromagnetic noise caused by electrical machinery, communication and control systems in the area and navigation and radio transmitters. This noise varies with time and so differencing transients at different times reveals this type of noise. In principle these sources should have low gradients over the MBUD receivers and should be canceled in the differencing process. It appears from the data in these tests that they are not canceled and improved filtering will be required to reduce their effect.

The transients obtained in the laboratory are labeled 'Land' on the plots and the transients obtained with the system on the sea bottom are labeled 'Marine'. The useful 'window' for transient measurement in these tests is from $3x10^{-4}$ sec to $4x10^{-2}$ sec.

The land transients are shown in Figures 35a, b and c for the Bx, By and Bz transmitters respectively. The target ball was only positioned at depths of 29, 43 and 57 cm. The target ball response falls below the noise level at greater depths. For the Bx transmitter the residual noise level is oscillatory and falls from about 10^{-12} volts per amp (V/A) at $4x10^{-3}$ sec to 10^{-13} V/A at 0.01 seconds. (The transients in all these plots are given in units of the voltage of the difference signal normalized by the peak transmitter current. They have not been converted to field strength). The target transient is above this noise in this same time range. For the By transmitter the residual noise is higher at $4x10^{-3}$ sec but falls rapidly to 10^{-13} V/A at $5x10^{-3}$ seconds. The target is easily seen at 57 cm and probably would have been seen even deeper. The residual noise level is even higher for the Bz transmitter and a crossover response is seen in the 5-7x 10^{-4} second range. Again, for this transmitter the target might have been seen at depths below the sea bottom greater than 57 cm at times greater $3x10^{-3}$ seconds. Simple extrapolation of the response versus depth indicates that the response would reach the noise level at about $5x10^{-3}$ seconds at a depth of approximately 150 cm below the bottom [about the expected depth of detection of a 152.4 mm sphere for BUD]. The target transients for the By and By transmitters do not display the early time crossover phenomena.

Land

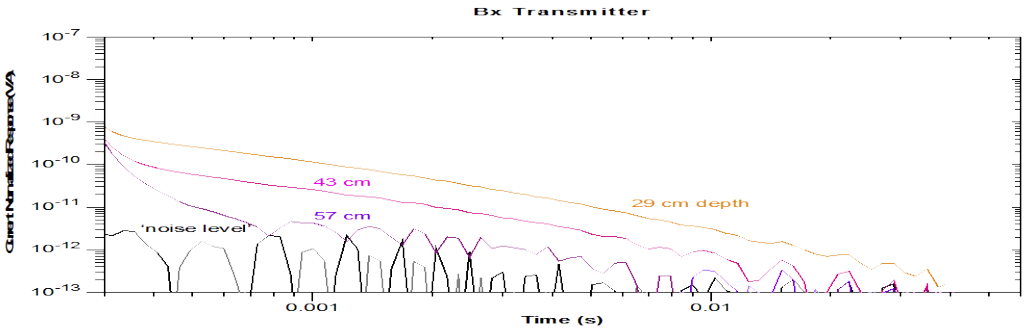

Figure 35a

Land

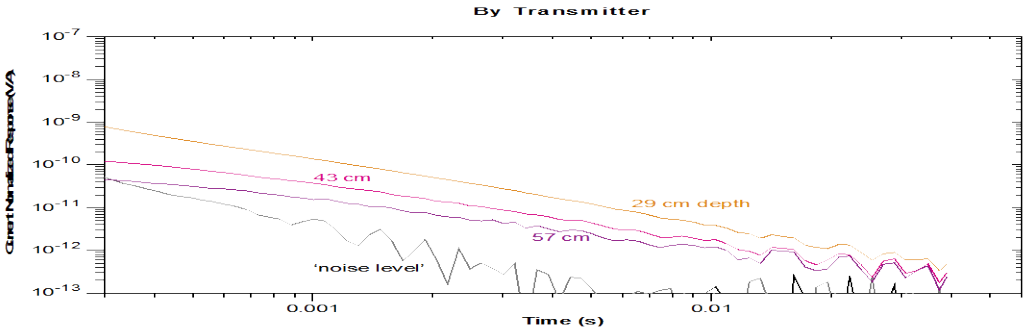

Figure 35b

Land

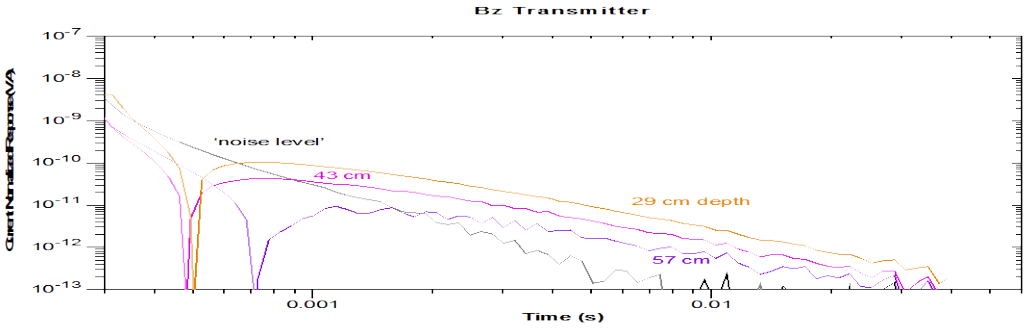

Figure 35c

The Marine transients are shown in figures 36a, b, c. A careful comparison of the transients in Figure 35 and 36 from the same transmitter shows that *the target transients at 29 and 43 cm depths are virtually identical for all transmitters for the land and marine data.* At 57 cm depth the ball response is affected by the noise and the transients are similar but not identical. *This shows that MBUD effectively cancels the seawater response and the sea-air interface response and yields the free-air target response.*

In detail these transients have a complicated form. The early time transients display the crossovers noted above for only some transmitters and at some depths. Without examining all the transmitter receiver combinations it is difficult to isolate the source of these effects. It is known that there were abundant metal scraps near the MBUD system in the laboratory and these could easily have coupled a secondary field into the system for some transmitter receiver geometries. The receiver data for all transmitters in the Marine tests display early time crossovers in the transients. It might be concluded that these are the characteristic effects of the induced electric dipole moments. As discussed above these moments are in general orthogonal to the induced magnetic moments and the secondary magnetic fields they produce at a receiver can be in the same direction as, orthogonal to or opposite to the secondary field from the magnetic induced moment. Without detailed modeling using all the transmitter combinations is difficult to ascribe a quantitative interpretation to these results.

It should be noted that the noise level is almost an order of magnitude higher in the Marine tests so the depth of detection is reduced. More testing of the system will be needed to identify the source of this background noise.

In summary the objective of this task and of the entire project, to show that MBUD could operate at shallow depth and cancel the seawater response through receiver differencing, has been met.

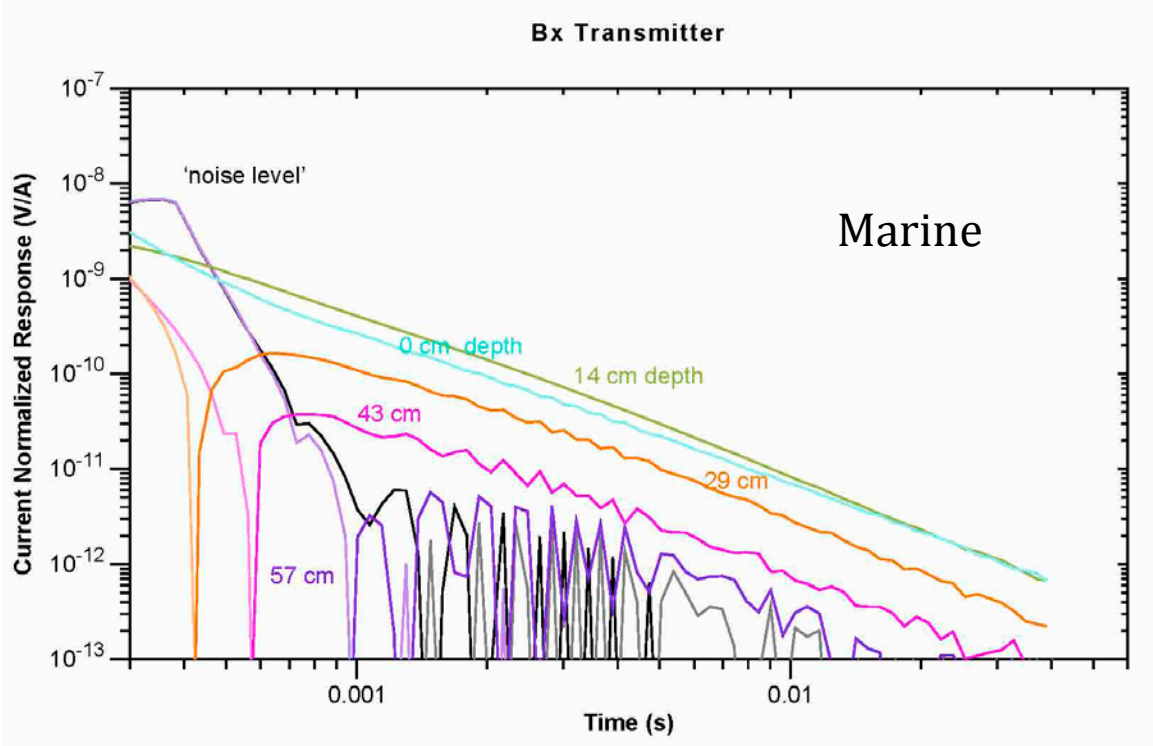

Figure 36a

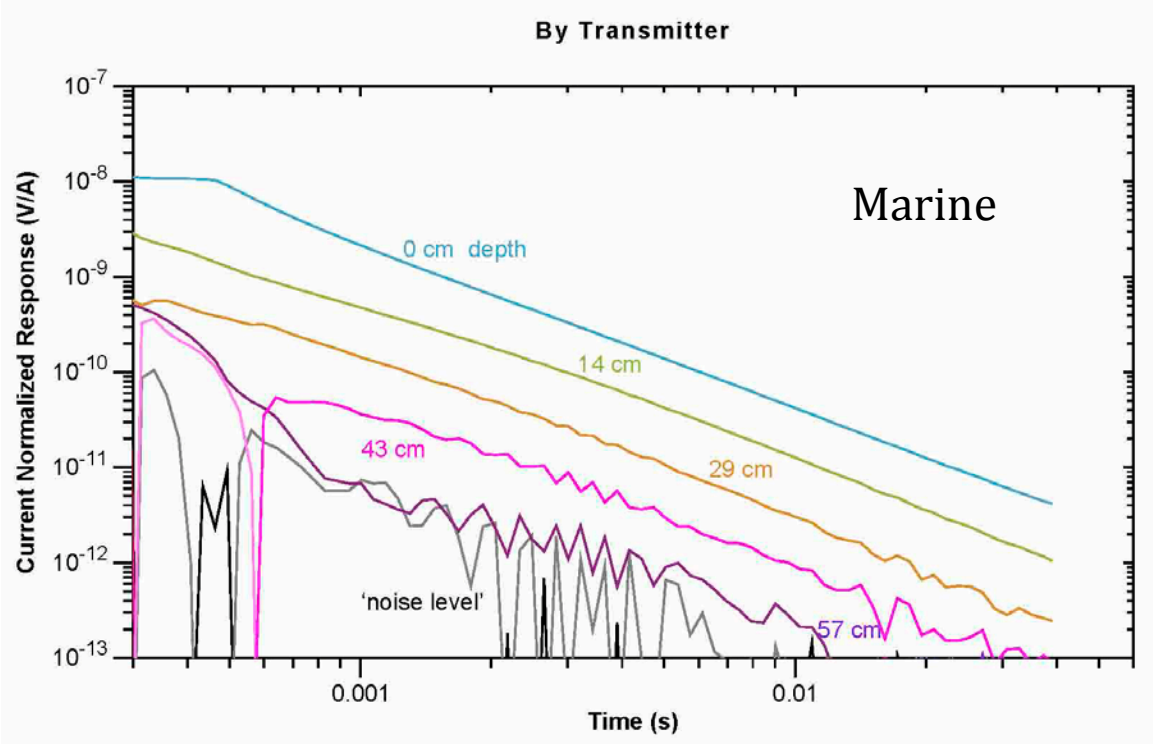

Figure 36b

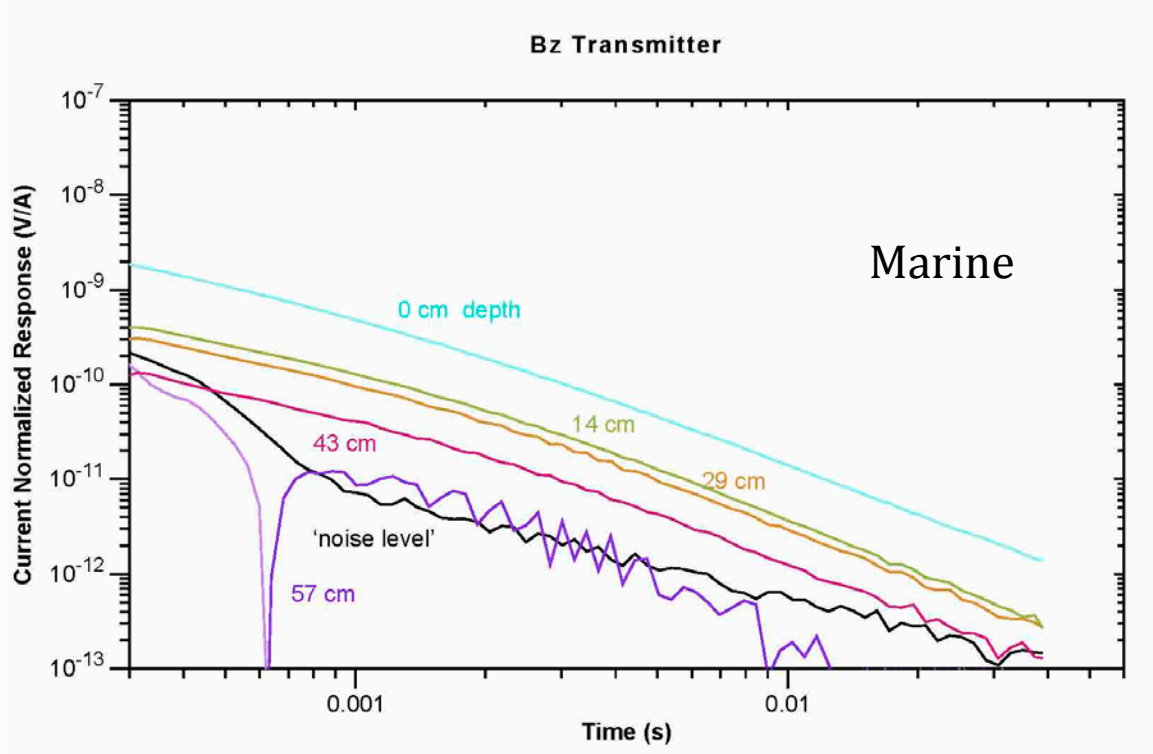
Bz Transmitter
Marine
0 cm depth
14 cm
29 cm
43 cm
'noise level'
57 cm
Current Normalized Response (V/A)
Time (s)
10-7
10-8
10-9
10-10
10-11
10-12
10-13
0.001
0.01

Figure 36c

Literature Cited.

1) Beche, J-F., Doolittle, L., Greer, J., Lafever, R., Zradding, A., Ratti, A., Yaver, S., Zimmermann, S., 2005, UXO Engineering Design: Technical Specification and Conceptual Design. Lawrence Berkeley National Laboratory – UXO Report to SERDP, April 2005

2) Gasperikova, E., Smith, J.T., Morrison, H.F., Becker, A., and Kappler, K, 2009, UXO detection and identification based on intrinsic target polarizabilities: Geophysics, 74, B1-B8.

3) Morrison, H.F., Alex Becker, Ugo Conti, and Erika Gasperikova, 2011, Ferrite-cored Solenoidal Induction Coil Sensor for BUD , June 30, 2011 LBL/SERDP Report (MM-1667).

4) Morrison, H.,F., U. Conti, V.F. Labson, E. Nichols, N.E. Goldstein, 1984, Field tests of Noise in Squid and Induction Coil Magnetometers, Report LBID-901, Earth Sciences Division, LBL, April 1984.

5) Smith, J.T.,Morrison, H.F., and Becker, A, 2004, Parametric forms and the inductive response of a permeable conducting sphere, J. Environ. and Engin. Geosci., **9**, 213-216.

6) Smith, J.T., and Morrison, H.F., 2004, Estimating equivalent dipole polarizabilities for the inductive response of isolated conductive bodies. I.E.E.E. Trans. Geosci. RemoteSensing, **42**, 1208-1214.

7) Smith, J.T., and Morrison, H.F., Becker, A., 2004, Resolution depths for some transmitter-receiver configurations: IEEE Trans. Geosci. Remote Sensing, **42**, 1215-1221.

8) Smith, J.T., and Morrison, H.F., 2005, Optimizing receiver configurations for resolution of equivalent dipole polarizabilities in-situ. I.E.E.E. Trans. Geosci RemoteSensing, **43**,1490-1498.

9) Smith, J.T., and Morrison, H.F., 2006, Approximating spheroid inductive responses using spheres: Geophysics, **71**, G21-25.

10) Smith, J.T., Morrison, H.F., Doolittle, L.R., and Tseng, H-W., 2007, Multi-transmitter null coupled systems for inductive detection and characterization of metallic objects:Journal of Applied Geophysics, **61**, 227–234.